Inhibiting stress corrosion cracking by removing corrosion products from the Mg-Zn-Zr alloy pre-exposed to corrosion solutions

Evgeniy Merson[1*], Vitaliy Poluyanov[1], Pavel Myagkikh[1], Dmitri Merson[1], Alexei Vinogradov[2]

[1]*Institute of Advanced Technologies, Togliatti State University, Belorusskaya str. 14, Togliatti 445667, Russian Federation*

[2]*Department of Mechanical and Industrial Engineering, Norwegian University of Science and Technology – NTNU, N-7491 Trondheim, Norway*

**Email: mersoned@gmail.com*

Magnesium and its alloys are susceptible to stress-corrosion cracking (SCC), which can manifest itself during the slow-strain rate tensile (SSRT) testing in air if the specimens were pre-exposed to corrosive media. This phenomenon is generally associated with hydrogen embrittlement (HE) which is believed to be related to diffusible hydrogen penetrating into the metal during the pre-exposure. In the present study, we show that the corrosion product layer deposited on the surface of the pre-exposed specimens is crucial in the SCC mechanism. The specimens of the alloy ZK60 were SSRT tested in air, in corrosive media, in air after pre-exposure to corrosive media as well as after pre-exposure and removal of corrosion products. To vary the severity of SCC, four NaCl-based corrosion solutions were utilised. The embrittlement resulted in a marked decrease in ductility and the concurrent appearance of multiple side-surface cracks as well as brittle fragments on the fracture surface. The most striking finding of the present study is that the removal of corrosion products from the surface of the pre-exposed specimens results in complete recovery of the mechanical response and in the elimination of all harmful embrittling features regardless of the corrosive solution used. This effect is found to be inconsistent with the common viewpoint where the SCC mechanism is governed entirely by diffusible hydrogen. The obtained results shed new light on the role of diffusible hydrogen, corrosion products and irreversible corrosion damage in the SCC mechanism of Mg alloys pre-exposed to corrosive media.

Keywords: magnesium alloys; stress-corrosion cracking; pre-exposure; corrosion products; hydrogen embrittlement.

1. Introduction

Metallic parts and structures exposed to the combined action of corrosive media and external stress suffer from stress corrosion cracking (SCC) to a larger or smaller extent [1]. SCC can lead to unpredictable catastrophic brittle failures at service stresses well below the yield strength. In particular, the wrought magnesium alloys are among the materials possessing relatively high susceptibility to SCC in a wide range of environments, including diluted NaCl solutions and even distilled water [2–4]. The poor resistance of Mg-based alloys to corrosion and SCC hinders their wider adoption by industry despite the growing attention paid by the engineering and research community to these materials in the past decades [5–8]. Due to their unrivalled strength-to-weight ratio, magnesium alloys are considered as potential candidates capable of replacing Al alloys and steels for manufacturing of lightweight components with ecological benefits and advantages of weight and cost savings in the automotive and aerospace industry [9–11]. An emerging application of Mg alloys is in the field of medicine striving to develop temporary supportive structures, such as implants and stents, which can be fully resorbed within a human body after the completion of the healing process without any adverse effects to the human body [12–16]. Since virtually any application of structural Mg alloys assumes temporal or permanent exposure to aggressive environment, the resistance of Mg alloys to corrosion and stress corrosion cracking is of vital importance for integrity and functionality of the entire component.

The development of SCC-resistant alloys requires an in-depth understanding of SCC, its mechanisms and evolution. Although this phenomenon has been extensively studied over the past few decades, the fundamental mechanism governing SCC of Mg is unclear as yet [2,3,17]. It has been generally accepted in the literature that besides the anodic dissolution (AD), which is chiefly responsible for the formation of the surface crack nuclei, hydrogen plays an essential role in the propagation of SCC cracks [18–21]. It is believed that atomic hydrogen evolved by the cathodic reaction on a metal surface during corrosion penetrates into the bulk metal and facilitates the crack growth through several possible hydrogen embrittlement (HE) mechanisms, which are commonly known as *hydrogen enhanced localised plasticity* (HELP), *hydrogen enhanced decohesion* (HEDE), *adsorption-induced dislocation emission* (AIDE) and *delayed hydride cracking* (DHC) [17,22–24]. The HELP mechanism implies that diffusible hydrogen, being accumulated at the crack tip, promotes ductile fracture by facilitating local dislocation movement. The presence of dimples on the fracture surfaces of AZ31, AZ91 and ZK60 was attributed to the dominance of the HELP mechanism in SCC of these alloys [18,25]. On the other hand, diffusible hydrogen is known to be capable of reduction of inter-atomic bond, thus

resulting in the enhancement of the brittle cleavage-like fracture through the HEDE mechanism. This mechanism is commonly recognised to be responsible for the brittle cleavage and intergranular facets on the fracture surfaces of Mg alloys subjected to SCC [18,25,26]. The AIDE mechanism is driven by the atomic hydrogen or other surface-active agents which are adsorbed at the inner surface of the crack tip [24,27]. It is suggested in this model that the adsorbed hydrogen weakens the interatomic bonds, alleviates the alternated dislocation emission from the crack tip and enhances the crack propagation, which is ductile by mechanism but is rather brittle in terms of resulting overall fracture surface appearance. The ample similarity between the fracture surface appearance in pure Mg fractured due to SCC and in liquid metal embrittlement cracking was considered as the evidence for the AIDE mechanism [27]. According to the DHC model, the SCC of Mg alloys can be related to the brittle hydrides, which are supposed to form at the crack tip due to interaction of Mg with hydrogen supplied to this region by diffusion through the metallic matrix or by adsorption at the crack surface and occlusion by the subsurface layer. SCC in Mg-Al [28–30], Mg-Al-Zn, Mg-Al-Mn [18,19] and Mg-Zn-Zr [25] was associated with the formation of brittle hydrides. Although all these mechanisms are persistently employed (individually or in various combinations) for the explanation of SCC of Mg alloys, there is still an obvious deficit of unambiguous evidence on the significance of specific SCC mechanisms in Mg-based alloys. In particular, an essential necessary condition for the operation of the HELP and HEDE mechanisms is the high concentration of diffusible hydrogen in the bulk metal. However, the results of the recent gas-analysis studies [31,32] cast substantial doubts on the significant occlusion of diffusible hydrogen by Mg alloys during SCC. It was shown that the concentration of diffusible hydrogen in the specimens of the alloys ZK60 and AZ31 and pure Mg subjected to SCC was not affected by the dislocation density [32] and/or the total grain boundary length [31], although both dislocations and grain boundaries are generally known as effective hydrogen traps. An important finding was that the concentration of diffusible hydrogen in the matrix was negligible after removing the corrosion products from the specimens embrittled due to SCC [32]. However, the specimens covered with corrosion products demonstrated considerable hydrogen desorption in the temperature range from 25 to 450 °C. The characteristic low-temperature extraction peaks could be potentially associated with diffusible hydrogen collected in the corrosion products layer. In the context of these findings, the role of the corrosion products layer in SCC of Mg cannot be underestimated and is of particular interest. Several studies have indicated that SCC of Mg and its alloys can be induced in the specimens by pre-exposure to corrosive media prior to tensile testing in air [28,33,34]. This phenomenon was unanimously explained by HE which was associated with the accumulation of diffusible hydrogen in the specimens during pre-exposure.

However, the role of the corrosion product layer deposited on the specimen's surface was not considered. Therefore, in the present study the specimens of ZK60 alloy pre-exposed to corrosion solutions of different chemical compositions were slow-strain rate tensile (SSRT) tested before and after removing corrosion products, to uncover the role of corrosion products film in the SCC mechanism in Mg alloys.

2. Experimental

2.1.Material and specimens

The commercial hot-extruded ZK60 alloy with the chemical composition provided in Table 1 was chosen as the model material for the present study. The material was the same as that used in the previous relevant studies [31,32,35]. In the as-received state, this alloy has a fine microstructure with average grain size of 3 μm [32].

Table 1 – Chemical composition of the alloy (in wt. %)

Material	**Mg**	**Al**	**Zn**	**Ca**	**Zr**	**Fe**	**Cu**	**Mn**	**Ce**	**Nd**	**Si**
ZK60	Balance	0.002	5.417	0.0004	0.471	0.001	0.002	0.005	0.002	0.003	0.003

Threaded specimens with the gauge parts of 30 mm length and 6 mm diameter were machined from the as-received extruded round bars of 25 mm diameter for the SSRT tests. The gauge parts of the specimens were grounded by SiC emery paper down to grade 2500. The mechanical properties of the specimens prepared from different as-received bars vary considerably, whereas the scatter of mechanical properties is insignificant for the specimens shaped from the same bar. Thus, if not stated otherwise, the experiments were carried out using the specimens made of the same bar.

For the corrosion rate measurements, gas-analysis and metallographic examination of the cross-sections, the samples of 15 mm length and 6 mm diameter were machined from the shoulder parts of the specimens fractured during mechanical tests.

2.2. Slow Strain Rate testing

The SSRT tests were conducted using the screw-driven frame AG-X Plus (Shimadzu) at $5.6 \cdot 10^{-6}$ s^{-1} (0.01 mm/min) strain rate. Four different conditions were implemented: (i) testing of reference specimens in air, (ii) testing in corrosive media, (iii) testing in air after pre-exposure to corrosive media and (iv) testing in air after pre-exposure to corrosive media and removing corrosion products. The corrosive solutions of four different chemical compositions were used -

(1) 0.1M (0.58 %) NaCl, (2) 4% NaCl + 4% K_2CrO_4, (3) 4% NaCl + 4% $K_2Cr_2O_7$, (4) 5 g/l (0.5 %) NaCl + 5 g/l (0.5 %) $K_2Cr_2O_7$ – according to [28,32,34,36] to vary the severity of SCC. During pre-exposure as well as during testing in corrosive media, the gauge part of a specimen was placed into the plexiglass cell filled with the corrosion solution contacting the specimen's surface at the open-circuit potential at 25±1 °C. The specimens were not loaded during the pre-exposure process. After 1.5 h of pre-exposure, the specimen was extracted from the corrosive solution, rinsed with cold water and ethanol, carefully dried with a paper towel and subjected to the SSRT testing either as is or after removal of corrosion products (referring to testing conditions "iii" and "iv", respectively). The relatively short time of pre-exposure in comparison to those commonly used in the other studies [28,33,34] was applied in the present work to minimise the irreversible corrosion damage produced by pre-exposure. Nevertheless, the effect of pre-exposure time will be considered separately in the forthcoming paper. The time lag between the end of pre-exposure and beginning of the SSRT test did not exceed 5 minutes. The removal of corrosion products was conducted by immersion of the specimen into the 20% CrO_3 +1%$AgNO_3$ aqueous solution for 1 min. Recently, we have confirmed that this procedure results in the complete removal of corrosion products from the specimen's surface, but it does not induce any noticeable damage to the bare metal [32].

2.3. Corrosion rate measurements

The corrosion rate was assessed by the weight loss method. The pre-exposure procedure for these samples was identical to that used for the specimens for the SSRT testing. After the end of the pre-exposure, the samples were extracted from corrosive media, rinsed with cold water and ethanol, carefully dried with a paper towel and then subjected to removal of corrosion products in the same way as it was done with the specimens for the SSRT testing. The weight, m, of each sample before, m_1, and right after pre-exposure, m_2, as well as after removal of corrosion products, m_3, were measured with ± 0.1 mg accuracy. The weight of corrosion products $m_{cp} = m_2 - m_3$ was estimated.

2.4.Gas-analysis

The thermal desorption spectroscopy (TDS) and hydrogen concentration measurements were conducted via the hot-extraction method in N_2 carrier gas flux using the G8 Galileo (Bruker) gas-analyser. The samples, which have been used for corrosion rate testing, were then subjected to the gas analysis in two states (i) after pre-exposure and (ii) after pre-exposure and removal of corrosion products. All samples were degreased with CCl_4 prior to testing. The gas-

analysis procedure was the same as that used in the previous studies [31,32] (see these references for details).

2.5. Microscopic analysis

The fractographic and side surface examination of the tested specimens was performed using a scanning electron microscopes (SEM) JCM-6000 (JEOL). The confocal laser scanning microscopy (CLSM), LEXT OLS4000 (Olympus) was used to measure the surface roughness induced by the corrosion process. For the cross-section analysis and evaluation of the corrosion products film thickness, the pre-exposed samples were cut in the transverse direction. They were then cold mounted in the epoxy resin, grounded and polished down with the final step done by the 0.25 μm water-free diamond suspension.

3. Results

3.1.Mechanical properties

Stress-strain diagrams, the average ultimate tensile stress (UTS) and elongation to failure (EF), are provided in Figs. 1 and 2, respectively, for the specimens tested under different conditions. As follows from these graphs, all specimens tested in corrosive media undergo severe embrittlement revealed by the dramatic drop of UTS and EF. The degree of embrittlement depends on the composition of the corrosion solution. The most significant reduction of elongation and strength is observed when the specimens are tested in 4% NaCl + 4% $K_2Cr_2O_7$ solution, c.f. Fig. 1d and 2a. In this media as well as in 4% NaCl + 4% K_2CrO_4 and 5 g/l NaCl + 5 g/l $K_2Cr_2O_7$ fracture always occurs at the quasi-elastic deformation region on the stress-strain diagram, see Fig. 1b-d. Among the investigated corrosive solutions, the 0.1M NaCl solution yields the smallest effect on mechanical properties. Nonetheless, the specimens fail just slightly beyond the yield point, c.f. Fig. 1a and 2a. Considering that the concentration of NaCl in 0.1M NaCl and 5 g/l NaCl + 5 g/l $K_2Cr_2O_7$ solutions is almost the same, one may conclude that the addition of passivating agents into corrosive media promotes SCC in the alloy ZK60. Furthermore, the comparison of mechanical properties of the specimens tested in 4% NaCl + 4% $K_2Cr_2O_7$ and 4% NaCl + 4% K_2CrO_4 solutions indicates that the addition of potassium dichromate is more deleterious for mechanical properties than the addition of potassium chromate. This result is in agreement with the literature data [36]. Finally, the obtained results indicate that the simultaneous increase in concentrations of both NaCl and $K_2Cr_2O_7$ enhances the SCC.

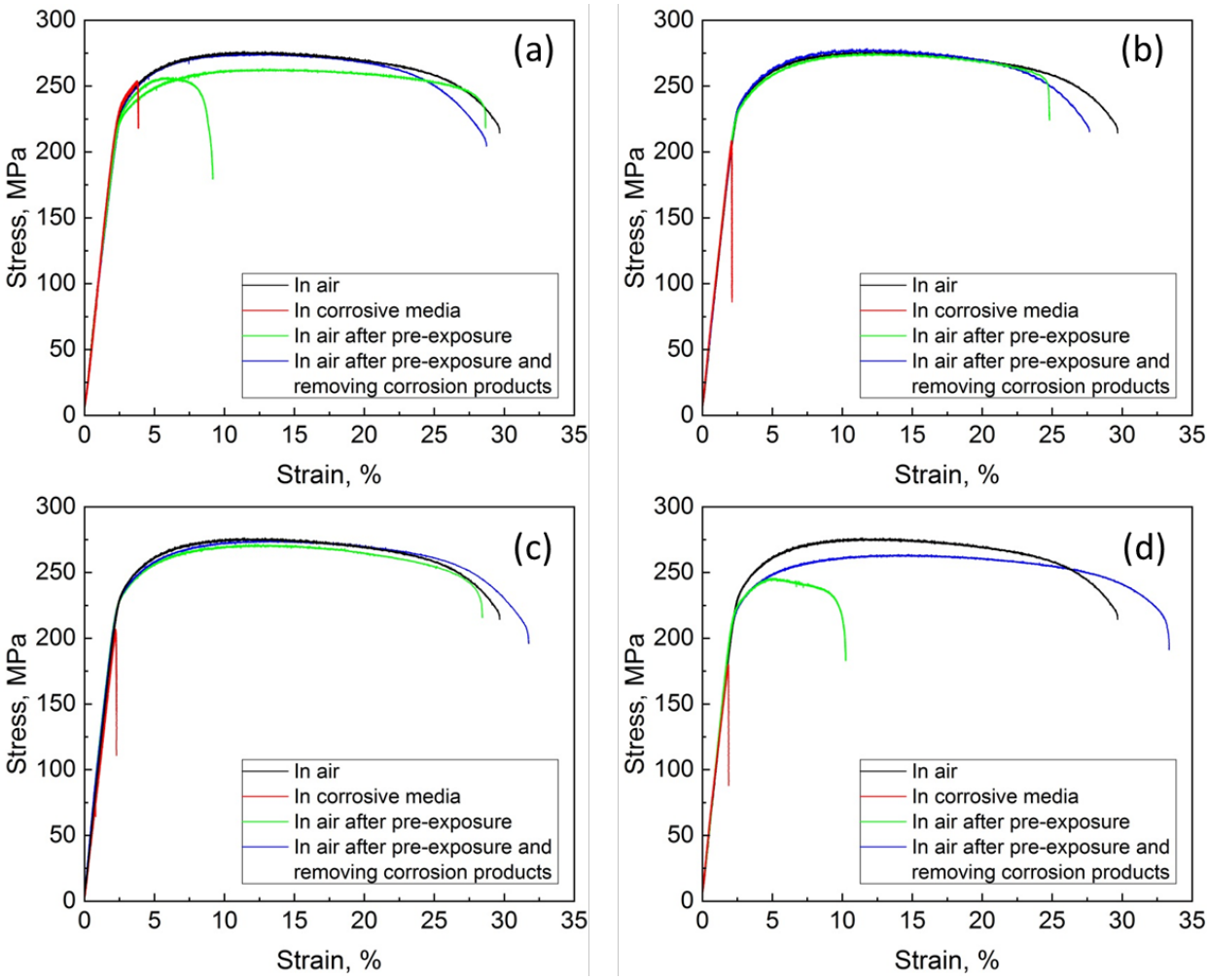

Fig. 1 – Stress-strain diagrams for the specimens made of the same bar of ZK60 alloy. The specimens were SSRT tested in air, in corrosive media, in air after pre-exposure to corrosive media or in air after pre-exposure to corrosive media and removal of corrosion products as shown in the legend. Chemical compositions of corrosive solutions are 0.1 M NaCl – (a), 4% NaCl + 4% K_2CrO_4 – (b), 5 g/l NaCl + 5 g/l $K_2Cr_2O_7$ – (c) and 4% NaCl + 4% $K_2Cr_2O_7$ – (d). Since only one of two specimens pre-exposed to 0.1 M NaCl solution suffered from the appreciable embrittlement, two green stress-strain curves are provided in Fig. 1a for both embrittled and ductile specimens.

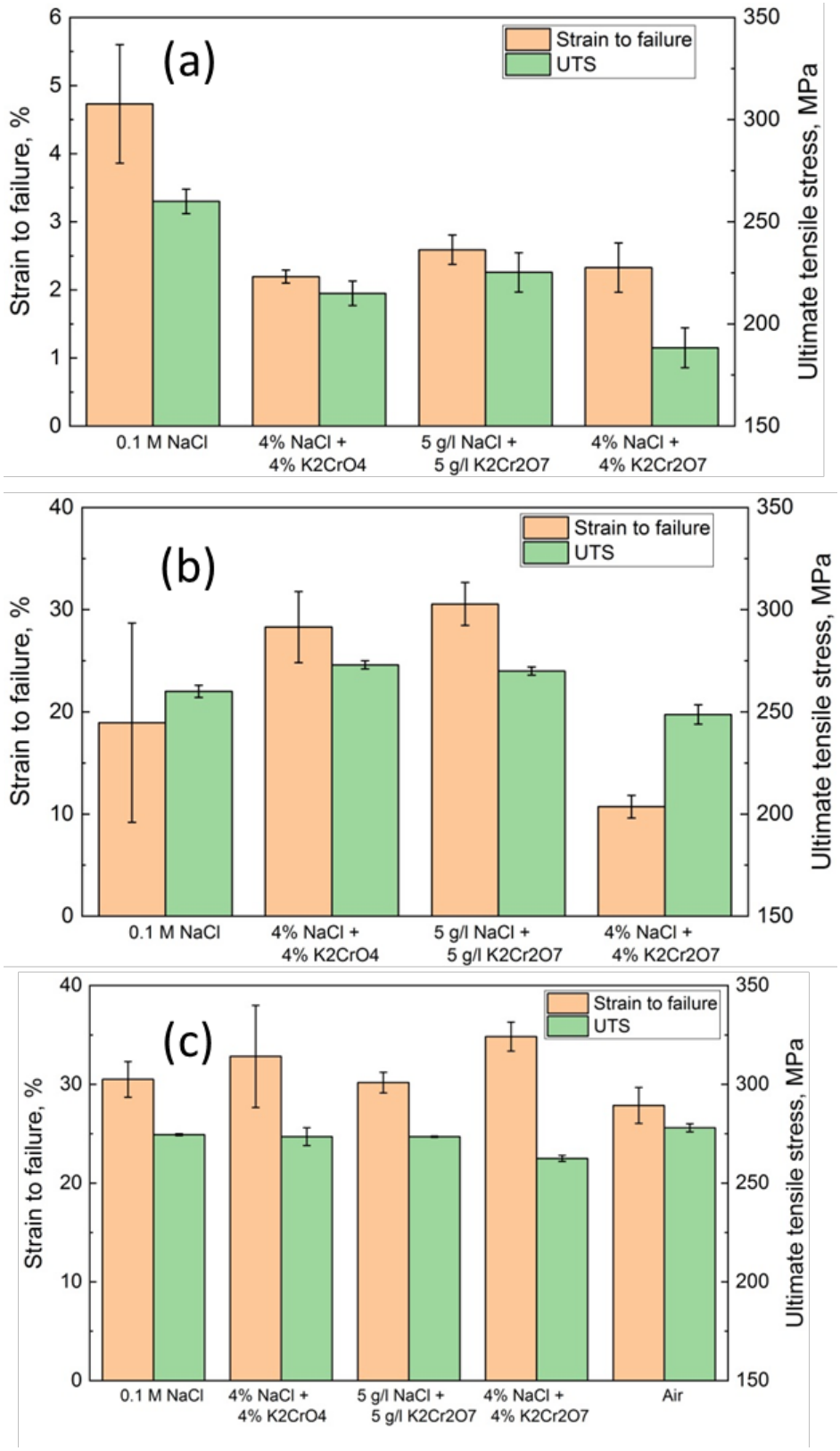

Fig. 2 – The ultimate tensile stress (UTS) and strain to failure (SF) average values for the specimens made of the same bar of ZK60 alloy and tested in corrosive media – (a), in air after pre-exposure to corrosive media – (b) and in air after pre-exposure to corrosive media and removal of corrosion products – (c). For the reference, the mechanical properties of the as-received specimens tested in air are shown in (c).

It can be seen in Fig. 1 and 2 that, on average, the ductility of the specimens tested in air after pre-exposure to corrosive media is lower than that of the specimens tested in air in the as-received state, but is higher than that of the specimens tested in corrosive media. Nevertheless, not all of the pre-exposed specimens exhibit perceptible embrittlement. In fact, the reproducible severe ductility loss is observed only after exposure of the specimens to the 4% NaCl + 4% $K_2Cr_2O_7$ solution, c. f. Fig. 1d and 2b. Just one specimen exposed to 0.1M NaCl and none of the specimens exposed to 4% NaCl + 4% K_2CrO_4 and to 5 g/l NaCl + 5 g/l $K_2Cr_2O_7$ demonstrate the substantial reduction of mechanical properties, c.f. Fig. 1a-c and 2b. The UTS value of the pre-exposed specimens is lower than that of the reference specimens, even in those cases when the elongation to failure was not affected significantly by the pre-exposure process. In contrast to the specimens tested in corrosive media, the pre-exposed specimens always fracture after considerable plastic strain with a minimum value around 10% which is recorded for the specimens pre-exposed to the 4% NaCl + 4% $K_2Cr_2O_7$ solution.

The most striking finding of the present study is that the ductility loss induced by pre-exposure to corrosive media can be fully recovered by the removal of corrosion products regardless of the composition of corrosive media used. It is evident from Fig. 1 and 2c that the EF value of the specimens tested in air after removal of corrosion products following pre-exposure to any corrosive media is of the same magnitude or even higher (!) than that of the reference specimens tested in air. None of the specimens with the removed corrosion products exhibit reduction in elongation. However, UTS of these specimens is commonly slightly lower than that of the reference specimens. Interestingly, that, among the specimens with removed corrosion products, the lowest UTS and the highest EF were observed in the specimens which were exposed to 4% NaCl + 4% $K_2Cr_2O_7$, i.e. those specimens which were contacting with media which results in the strongest ductility-loss effect when corrosion products are retained on the surface of the specimen.

For higher confidence and easy comprehension, the summary plot representing more significant statistics is provided in Fig. 3. Each experimental point represents the UTS and EF values for one specimen tested under the specific experimental condition (colour- and shape-coded on the graph). The data represented in Fig. 3 were obtained using the specimens made from different bars of the same ZK60 alloy. The considerable scattering in mechanical properties in the as-received state, c.f. black dots in Fig. 3, is caused, probably by the variations in the microstructure due to undocumented variations in the hot extrusion processing. This variance, however, does not change the common trends. Figure 3 shows that: (i) all specimens tested in corrosive media are embrittled severely; (ii) all specimens tested in air after pre-exposure to 4%

NaCl + 4% $K_2Cr_2O_7$ suffer from significant embrittlement, albeit to a lesser degree than that for the specimens tested in corrosive media; (iii) pre-exposure of the specimens to any other corrosive solution, as a rule, does not lead to considerable embrittlement, though their mechanical properties in air are slightly lower on average than in the as-received state; (iv) none of the specimens tested in air after removal of corrosion products deposited on the specimen's surface upon submersion to corrosive media exhibits any signature of embrittlement, regardless of the chemical composition of the corrosive solution used. The corollary for these systematic observations is that the corrosion products retaining on the specimen's surface after pre-exposure to corrosive media play a significant, if not a central role, in the embrittlement mechanism of Mg alloys.

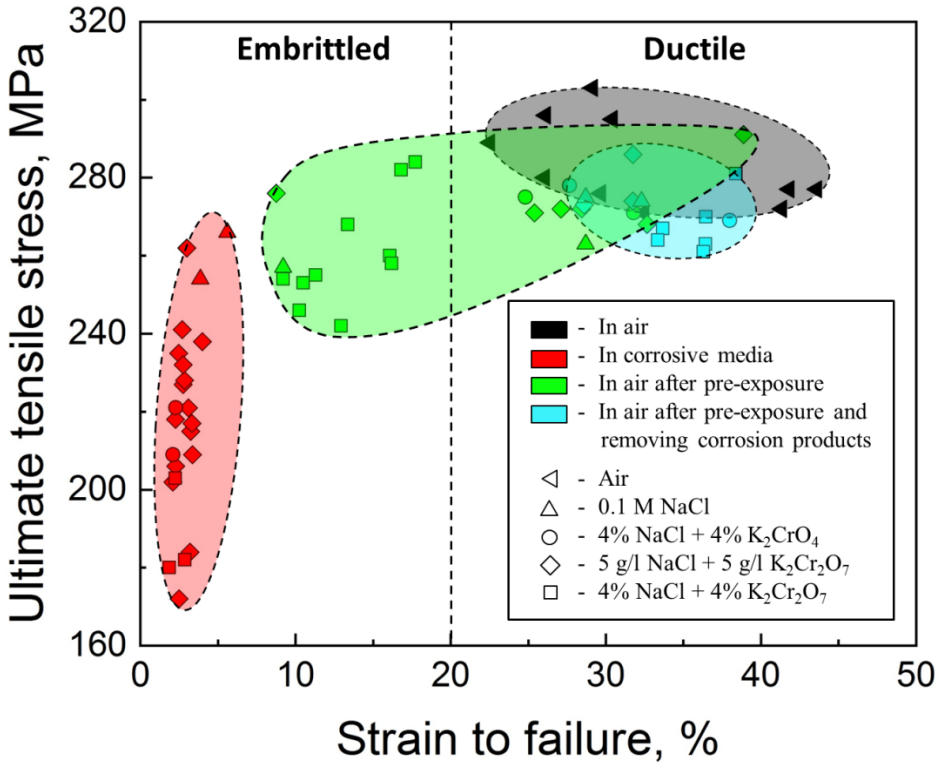

Fig 3 – The UTS and SF values for the specimens SSRT tested under different conditions and in different media. The experimental points represented on the plot correspond to similar specimens machined from different bars of the ZK60 alloy.

3.2.Side surface examination

Side surfaces of the specimens tested in corrosive media or tested in air after pre-exposure to corrosive media are covered by corrosion products. The morphological features of the corrosion product layer depend on the chemical composition of the corrosion solution, c.f. Fig. 4 and 5. Specimens which were exposed to, or tested in, the 4% NaCl + 4% $K_2Cr_2O_7$ solution are entirely covered by a solid layer of dark corrosion products. Although corrosion products on the

surface of the specimens exposed to 5 g/l NaCl + 5 g/l $K_2Cr_2O_7$ and 4% NaCl + 4% K_2CrO_4 solutions are also dark, they have the lower hiding power compared to those of the specimens exposed to 4% NaCl + 4% $K_2Cr_2O_7$. Corrosion products on the surface of the specimens contacted with the 4% NaCl + 4% K_2CrO_4 solution are presented by just a few dark stains, while the rest of the gauge surface remains virtually intact by corrosion. The specimens, which have beed tested in 0.1M NaCl, are well-covered with a layer of grey corrosion products. Thus, the dark colour of the corrosion products is associated with the presence of potassium chromate or dichromate in the corrosion solution. After pre-exposure to the 0.1M NaCl solution, the specimen's surface is less covered by corrosion products than after testing in the same solution so that one can see some bright spots revealing fragments of the bare metal. After the chemical removal of corrosion products, the side surface of all specimens becomes matt and grey in the areas which were occupied by corrosion products, while intact regions remain shiny.

To assess the specimens' ductility, one can use photographs presented in Fig. 4 by their thickness and length after testing. For example, it is obvious that the fracture of the specimens with removed corrosion products was preceded by a sizable amount of plastic deformation and pronounced necking. In contrast, the specimens tested in corrosive media fractured in a brittle manner with the absence of visible necking. The similar brittle fracture features correspond to all specimens after pre-exposure to the 4% NaCl + 4% $K_2Cr_2O_7$ solution. These features are observed concomitantly with a substantial drop in mechanical properties. The other pre-exposed specimens were fractured with the formation of saw-teeth shear lips, moderate necking and appreciable elongation as can be seen in Fig. 4.

The areal roughness of the specimen’s side surface was measured using the CLSM. As can be seen on the histogram provided in Fig. 6, the root mean square height - Sq - of the surface relief is the highest for the specimens interacted with the 4% NaCl + 4% $K_2Cr_2O_7$ solution, including the specimens with removed corrosion products. Obviously, these specimens underwent much more severe corrosion damage during pre-exposure if compared to the specimens pre-exposed to other corrosive solutions. This observation can probably explain the irreversible reduction of UTS in these specimens after removal of corrosion products. The corrosion damage produced by other corrosive solutions is likely too low to establish any relationship between the mechanical properties of the specimens and the surface roughness.

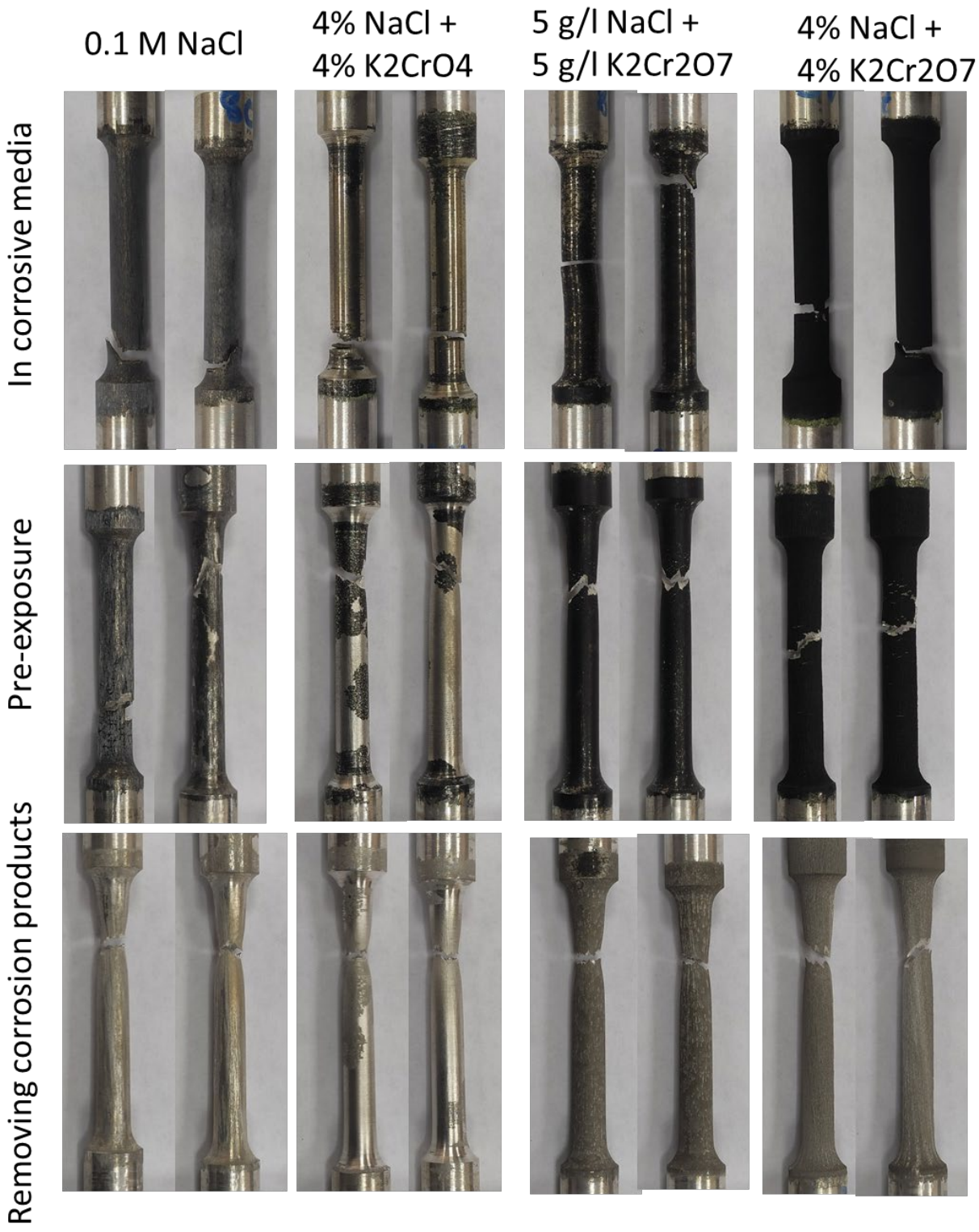

Fig. 4 – The appearance of the specimens made of the same bar of ZK60 alloy and SSRT tested at different experimental conditions and corrosive environments.

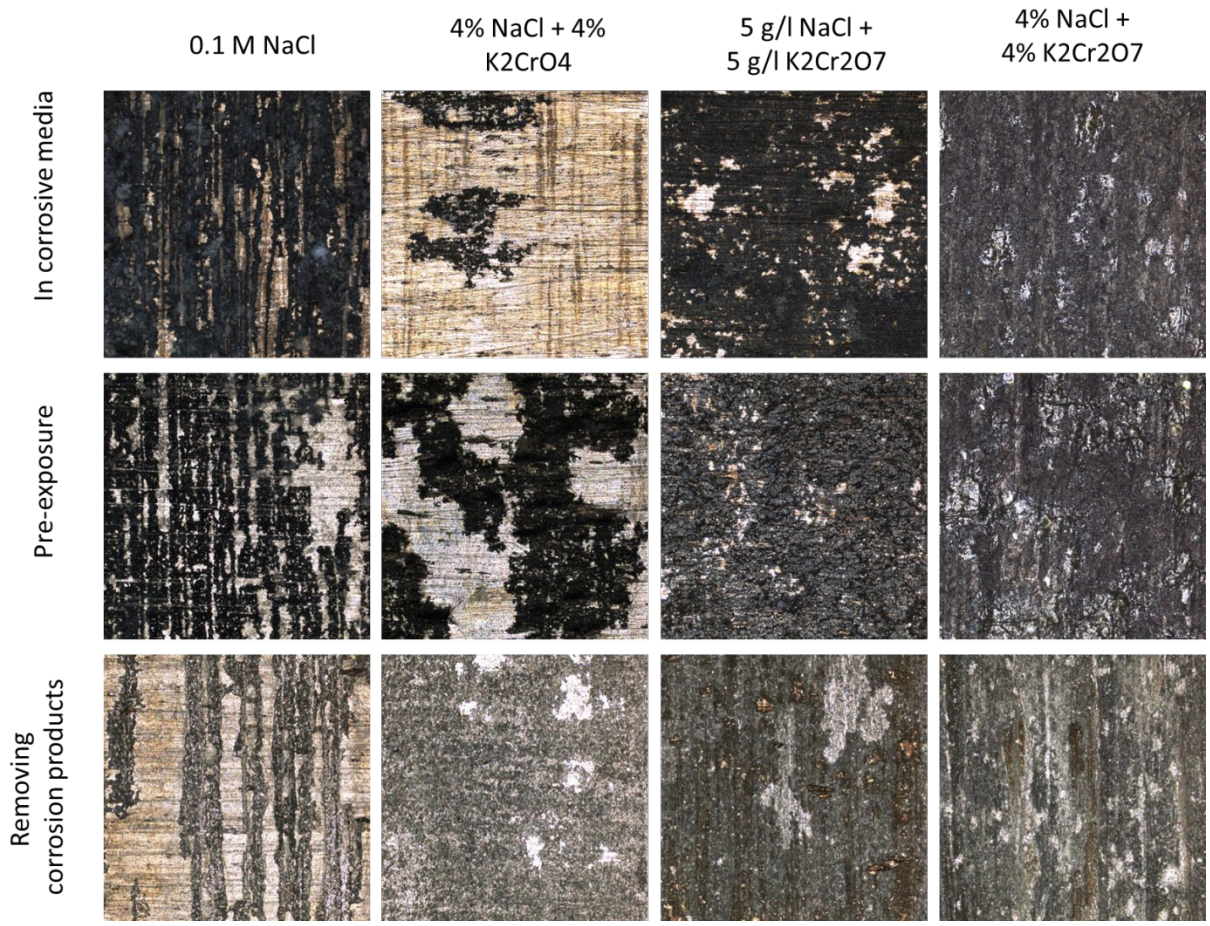

Fig. 5 – The CLSM images of the side surface of the specimens made of the same bar of ZK60 alloy and SSRT tested at different experimental conditions and corrosive environments

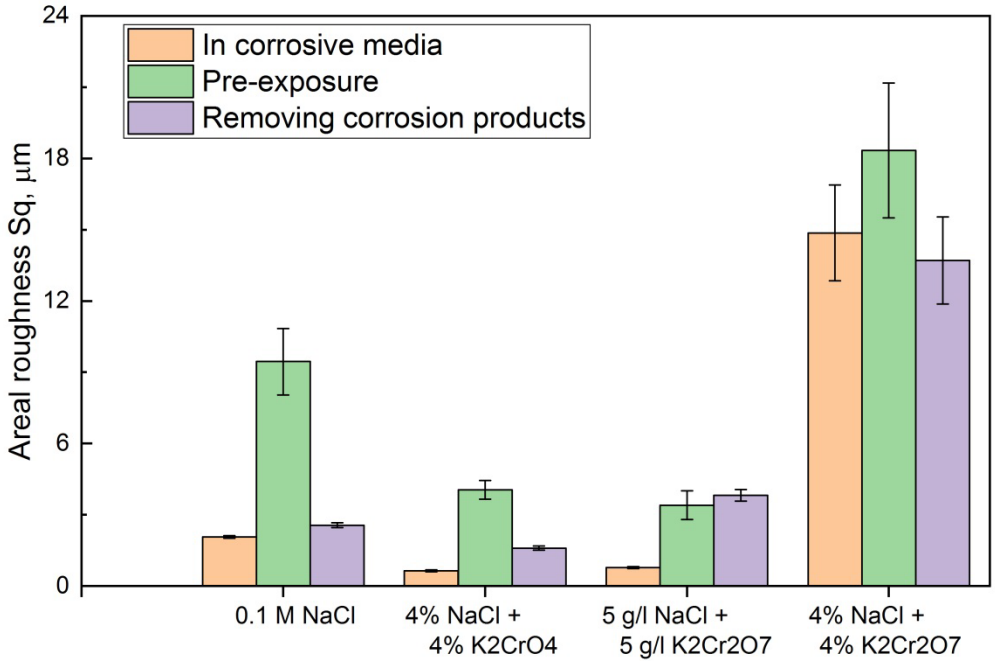

Fig. 6 – The areal roughness in terms of root mean square profile height – Sq for the specimens interacted with different corrosive solutions during the SSRT testing or during pre-exposure.

Secondary macro- and microcracks are found on the side surface of the specimens, which were tested in corrosive media as well as after pre-exposure to corrosive media. As opposed to this, no secondary cracks have been observed on the surface of the specimens which were tested in air after removal of corrosion products. The specimens tested in corrosive solutions commonly contain a few long and deep cracks, located close to the fracture surface, c.f. Fig. 7. It is interesting that the cracks in the specimens tested in 4% NaCl + 4% $K_2Cr_2O_7$ exhibit the characteristic S-shape, Fig. 7b, which resembles that of the cracks produced in low-carbon steel due to hydrogen embrittlement during tensile testing with in-situ cathodic hydrogen charging [37,38].

Pre-exposed and SSRT-tested specimens are featured by a notably larger number of cracks, which are uniformly distributed along the entire surface of their gauge parts, c.f. Fig. 8 and 9. It can be clearly seen on SEM images in Fig. 8a-c and on the CLSM profile maps in Fig. 9a-c, that even the specimens, which were not severely embrittled (e.g. those pre-exposed to 0.1 M NaCl, 4% NaCl + 4% K_2CrO_4 and 5 g/l NaCl + 5 g/l $K_2Cr_2O_7$), contain many considerably opened cracks. However, the SEM observations at higher magnification show that these cracks are blunted and exhibit a rough ductile fracture surface relief, Fig. 8a-c. In contrast, the cracks on the specimens embrittled in the 4% NaCl + 4% $K_2Cr_2O_7$ solution are more deep, sharp and brittle in their appearance, Figs. 8d and 9. Beside the macro-cracks, one can notice a dense network of brittle micro-cracks covering the surface of the specimens tested in air after submersion in aggressive media.

Apparently, the environmentally-induced secondary cracks nucleate due to brittle fracture of the corrosion product layer which has been deposited on the surface either during pre-exposure or during testing in aggressive media. However, in the specimens, which have not been embrittled strongly after pre-exposure, these cracks can blunt and cease to propagate deeply into the bulk. In contrast, in the embrittled specimens such as those pre-exposed to 4% NaCl + 4% $K_2Cr_2O_7$ or those tested in corrosive solutions, the cracks nucleated in the corrosion product layer and propagated to the bulk in a brittle manner. Thus, the similarity between the embrittled specimens tested in corrosive media and those tested in air after pre-exposure is that there are the mechanisms inhibiting local plasticity and crack tip blunting and promoting brittle fracture. Obviously, those mechanisms are irrelevant when the corrosion product layer is absent, i.e. when the environmentally-induced cracks cannot initiate.

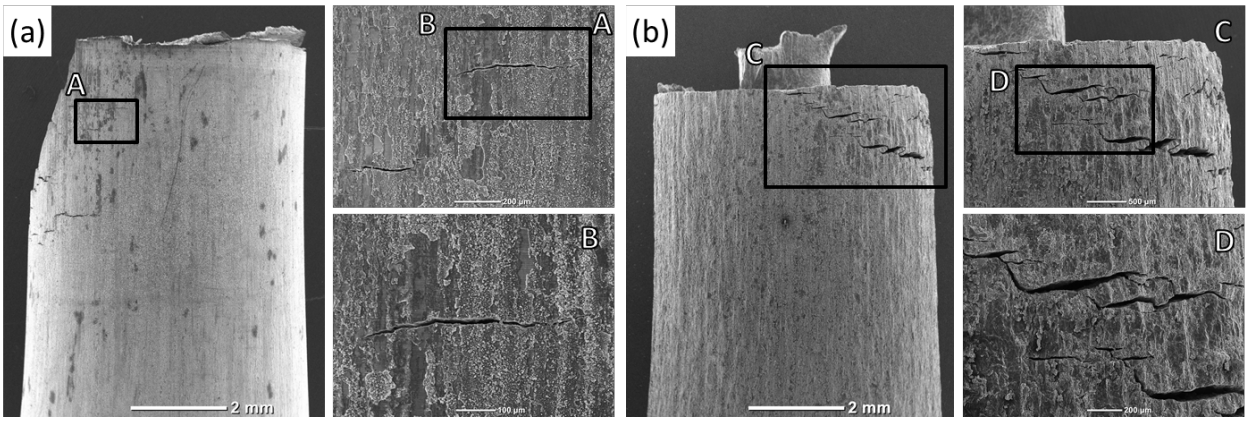

Fig. 7 – The SEM images representing the side surface of the specimens SSRT tested in 0.1 M NaCl – (a) and 4% NaCl + 4% $K_2Cr_2O_7$ – (b) solutions

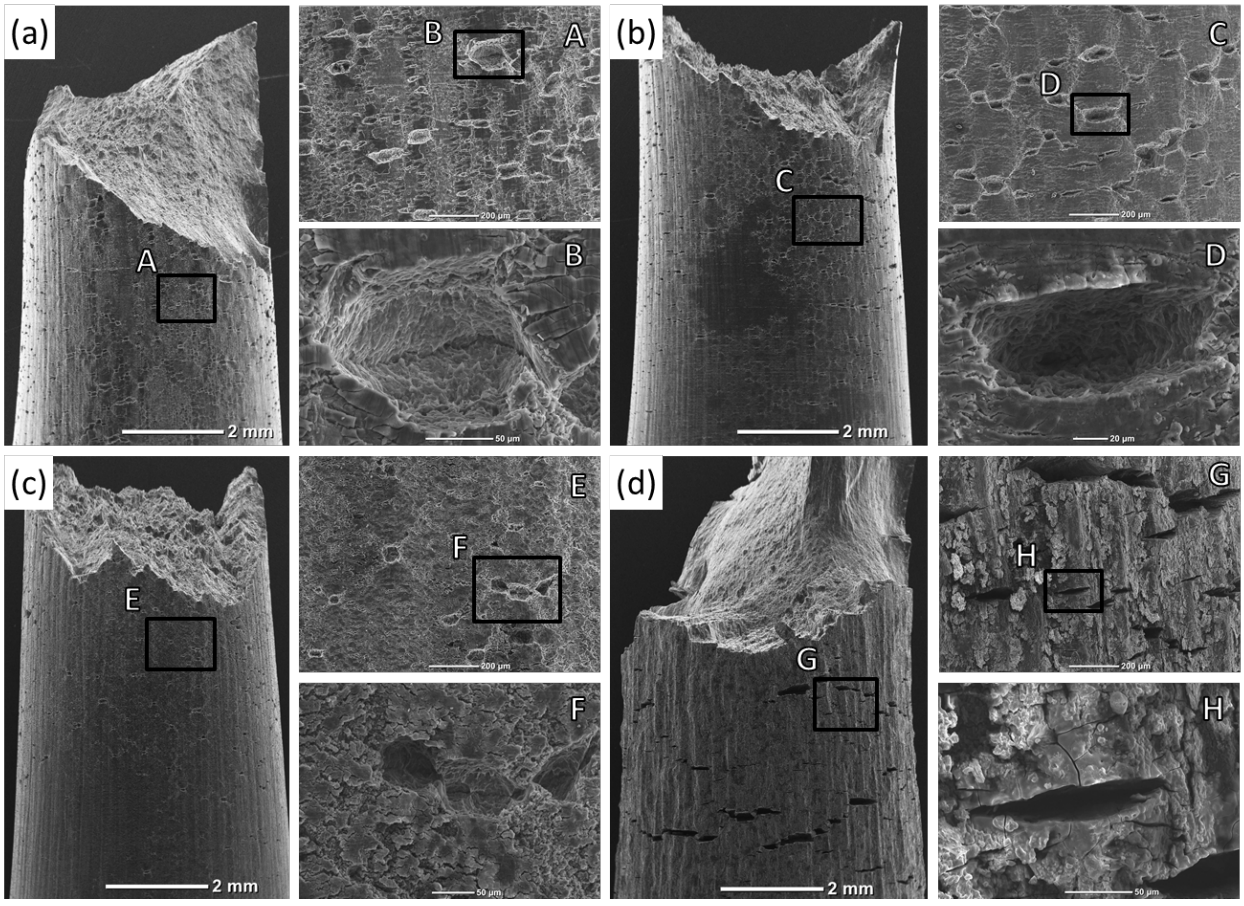

Fig. 8 – The SEM images representing the side surface of the specimens SSRT tested in air after pre-exposure to 0.1 M NaCl – (a), 4% NaCl + 4% K_2CrO_4 – (b) and 5 g/l NaCl + 5 g/l $K_2Cr_2O_7$ – (c), 4% NaCl + 4% $K_2Cr_2O_7$ – (d) solutions.

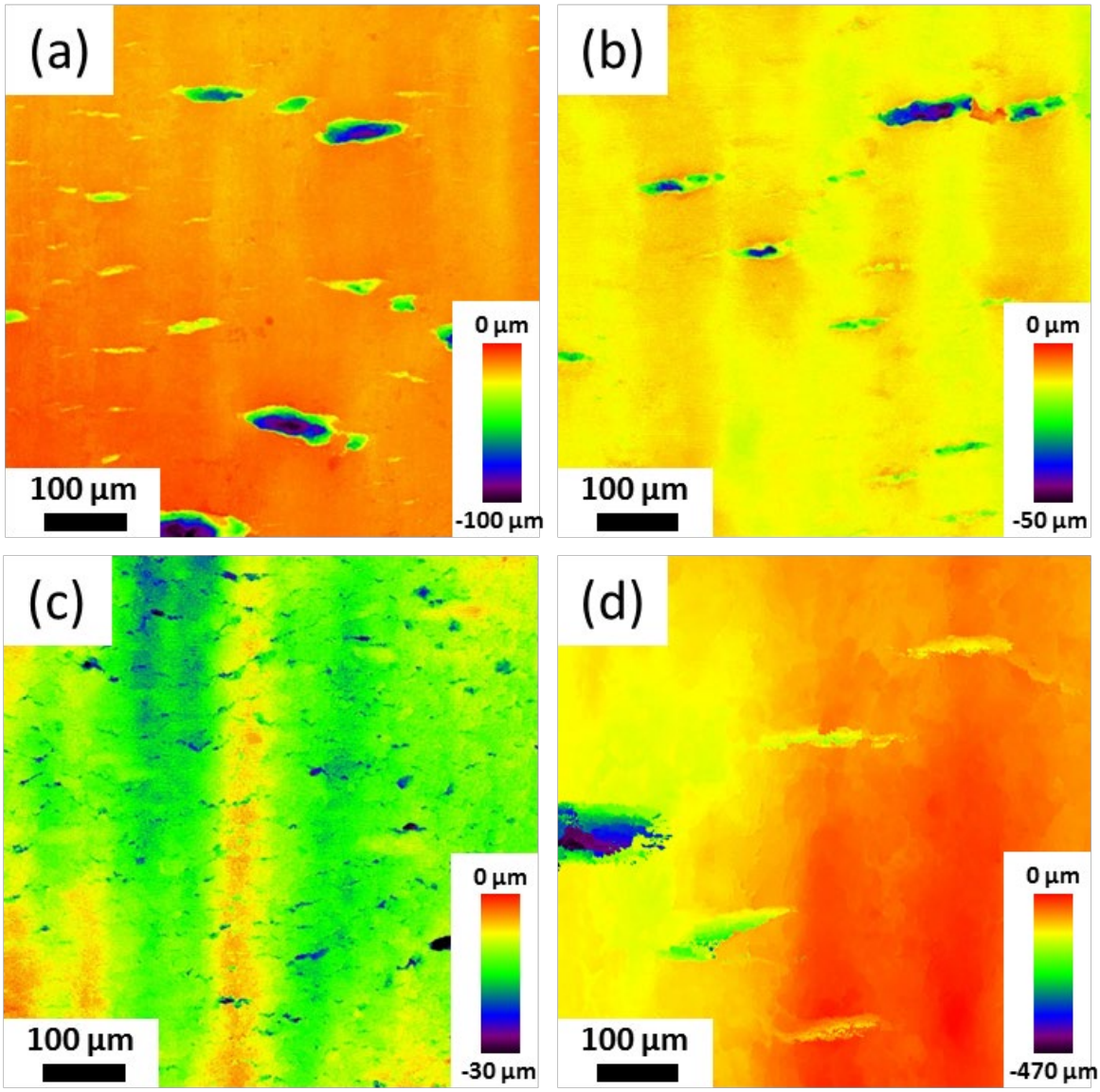

Fig. 9 – The CLSM height maps of the side surface of the SSRT-tested specimens pre-exposed to 0.1 M NaCl – (a), 4% NaCl + 4% K_2CrO_4 – (b) and 5 g/l NaCl + 5 g/l $K_2Cr_2O_7$ – (c), 4% NaCl + 4% $K_2Cr_2O_7$ – (d) solutions.

3.3.Fractographic examination

The fracture surfaces of the specimens which were tested in corrosive media or in air after pre-exposure to corrosive media demonstrate a mixed brittle/ductile appearance, c.f. Fig. 10. In comparison to the pre-exposed ones, the specimens tested in corrosive media exhibit a much larger area of brittle fragments on the fracture surface. Figure 10 reveals that the fracture in these specimens occurred primarily by the growth of a dominating crack followed by the final ductile rupture. Six characteristic regions following one another can be distinguished on the fracture surfaces of the specimens tested in corrosive media as indicated, for an example, by letter-labelled arrows in Fig. 10 for the specimen tested in 5 g/l NaCl + 5 g/l $K_2Cr_2O_7$. As is illustrated

by Fig. 11, each of these regions has a distinct morphology: (i) corrosion products film at the edge of the fracture surface, Fig. 11a, (ii) intergranular and cleavage facets, Fig. 11b, (iii) fluted facets, Fig. 11c, (iv) fluted facets with secondary cracks, Fig. 11d, (v) flat dimpled, Fig. 11e, and (vi) slant dimpled reliefs, Fig. 11f. In the present study, the part of the fracture surface composed of the first four zones is referred to as a "brittle component", while a “ductile component” denotes the part of the fracture surface with the prevailing morphologies (v) and (vi). The detailed discussion on the morphological features typifying these zones is beyond the scope of the present study and can be found elsewhere [35].

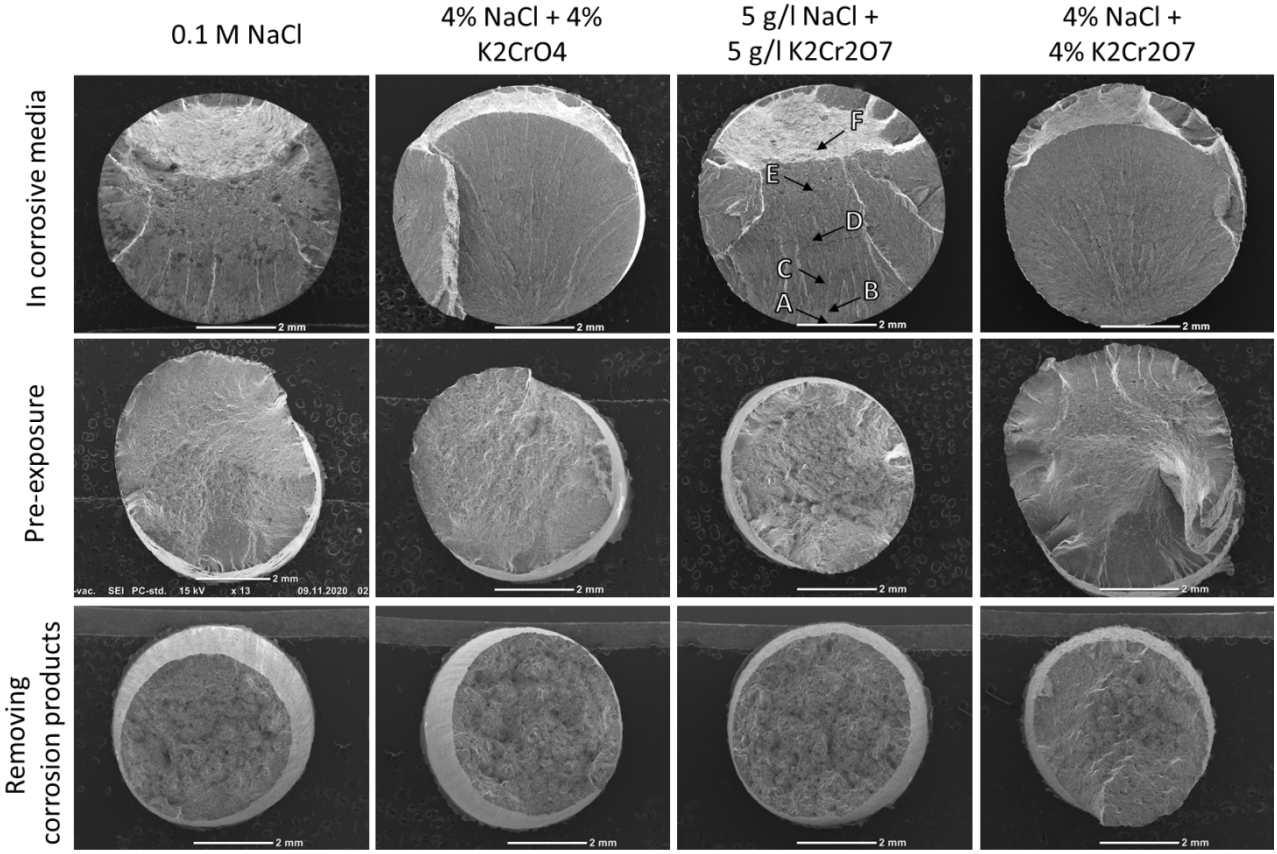

Fig. 10 – The SEM images representing the entire fracture surfaces of the specimens of ZK60 alloy SSRT tested in different corrosive environments and testing conditions. The arrows with corresponding designations indicate the location of characteristic regions, the morphology of which is represented in Fig. 11.

In contrast to the specimens tested in corrosive solutions, the pre-exposed ones exhibit the annular brittle zone and ductile morphology in the central part of the fracture surface, Fig. 10 and 12a. When viewed from a side angle, the annular brittle zone appears as a screw-like twisted surface with step-like terraces, Fig. 12a, which were obviously produced by multiple individual

side surface cracks like those observed by side surface examination, Figs. 8 and 9. These cracks, nucleating and propagating along the gauge part of the specimen, finally, coalesce, thus producing the characteristic fracture surface represented in Fig. 12a. It should be noted that, among the pre-exposed specimens, the well-defined brittle zone is observed only in the specimens which do exhibit significant embrittlement. The fracture surface of such specimens is represented by the morphologies which are similar to those in the specimens tested in corrosive solutions. However, the area of the edge regions covered by corrosion products in the pre-exposed specimens is notably larger, Fig. 12b. Morphological details of these featureless regions are masked under the cracked dense layer of corrosion products, Fig. 12c. Along the crack path, the featureless regions are followed by the brittle cleavage and intergranular facets, which appearance suggests that they were damaged by corrosion, Fig. 12d. The subsequent zones of fluted facets and flat dimpled fracture have pretty much the same morphology as that of the specimens tested in corrosive media, Figs. 12e and f, though the fluted region with secondary cracks is absent in the pre-exposed specimens. As can be seen in Fig. 13, the fracture surfaces of the pre-exposed specimens, which do not undergo substantial embrittlement, e.g. the ones pre-exposed to the 5 g/l NaCl + 5 g/l $K_2Cr_2O_7$ and 4% NaCl + 4% K_2CrO_4 solutions, are mostly ductile. Nonetheless, many featureless regions with corrosion products are presented at the edge of the fracture surface of these specimens, Fig. 13.

In excellent agreement with the other results of the present study, all pre-corroded specimens which were tested in air after removal of corrosion products have completely ductile dimpled fracture surface without any signs of brittle fracture morphology regardless of the composition of the corrosion media used, Fig. 10. The appearance of the fracture surface of these specimens is very similar to that of the reference specimens tested in air.

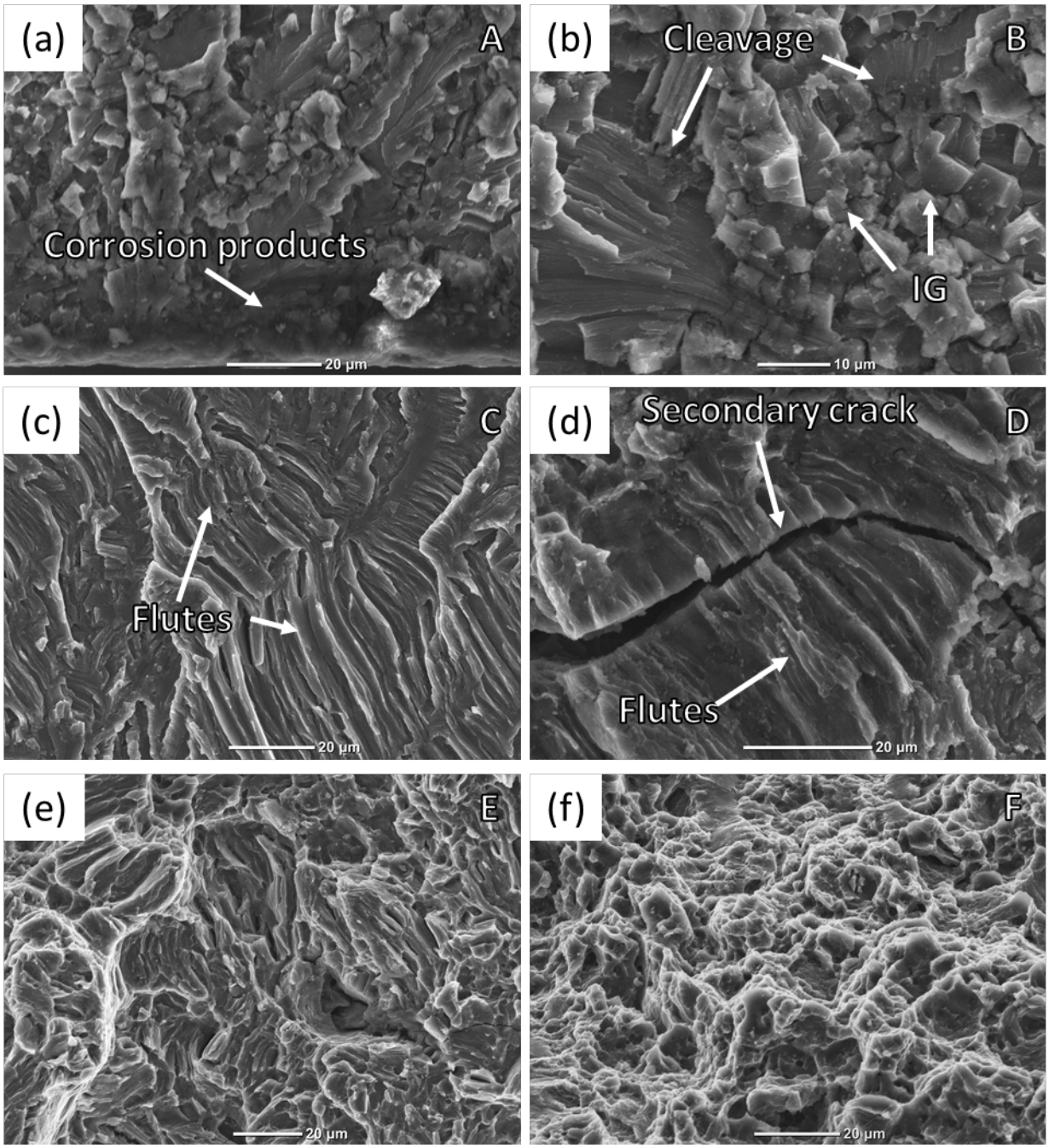

Fig. 11 - The SEM images representing the characteristic fracture surface morphologies of the specimen SSRT tested in 5 g/l NaCl + 5 g/l $K_2Cr_2O_7$ solution. The location of the regions on figures a-f, is indicated by the arrows latter-labelled as "A-F" in Fig. 10.

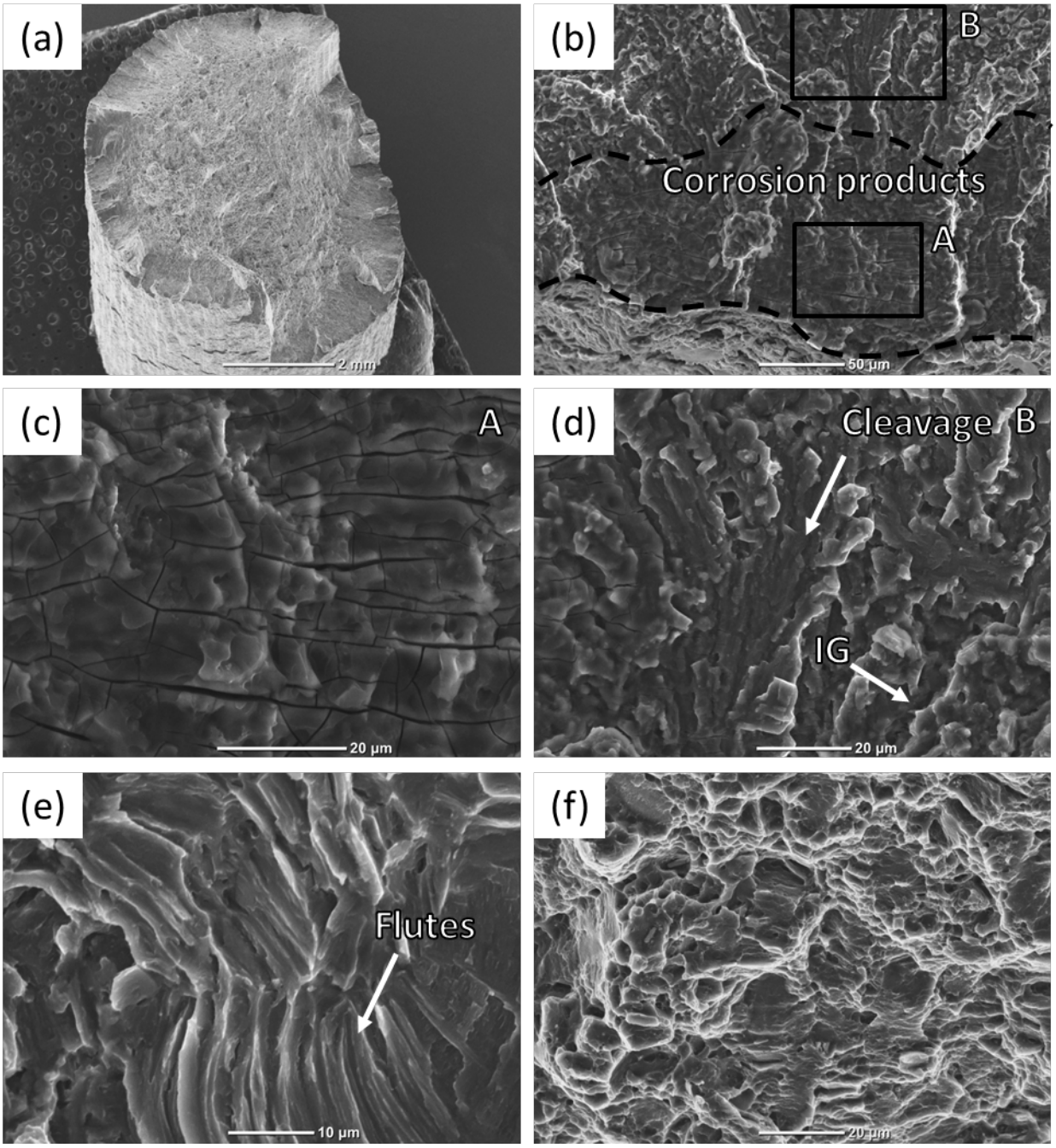

Fig. 12 – The SEM images representing the characteristic fracture surface morphologies of the specimen SSRT tested in air after pre-exposure to 4% NaCl + 4% $K_2Cr_2O_7$ solution: (a) – side view of entire fracture surface; (b) – featureless region covered by corrosion products at the edge of the fracture surface; (c) – the magnified region marked by "A" in (b); (d) – the magnified region marked by "B" in (b), representing the cleavage and intergranular facets damaged by corrosion; (e) - the fluted morphology next to the cleavage and intergranular region; (f) – dimpled relief in the central part of the fracture surface.

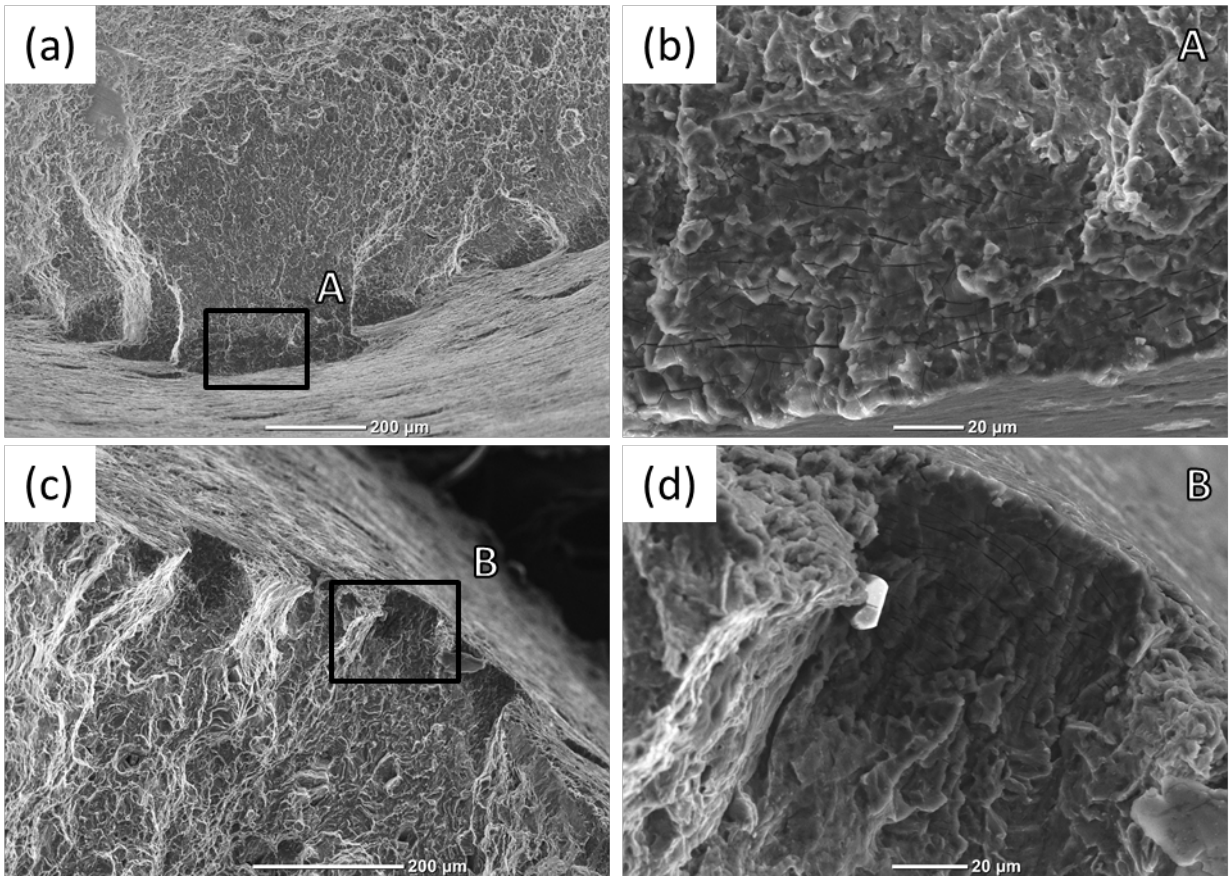

Fig. 13 - The SEM images representing the close-to-side surface fragments of fracture surface of the not embrittled specimens pre-exposed to the 4% NaCl + 4% K_2CrO_4 – (a, b) and 5 g/l NaCl + 5 g/l $K_2Cr_2O_7$ – (c, d) solutions. The magnified regions marked by A and B in (a) and (c) are represented in (b) and (d), respectively.

3.4.Corrosion rate measurements

Since the results of the SSRT testing indicated the existence of the strong relationship between the corrosion behaviour of the alloy and its susceptibility to pre-exposure embrittlement, the additional experiments on the small cylindrical samples of the same alloy were performed to assess the corrosion rate and characteristics of the corrosion products layer in different solutions and, thus, to quantify the observed relationship.

The corrosion rates measured by the weight loss method after 1.5 h pre-exposure of the samples to the different corrosion solutions are represented in Fig. 14. It can be seen that the corrosion rate of the alloy in the 4% NaCl + 4% $K_2Cr_2O_7$ solution, which is the only one producing the persistent pre-exposure embrittlement, is extremely high and is an order of magnitude higher than in the other solutions. Pre-exposure to this solution reasonably results in the production of a large amount of corrosion products as is indicated by their weight, Fig. 14, and thickness assessed by the side surface observations, Fig. 14, 15. The corrosion rate and

weight of the corrosion products produced in the 0.1 M NaCl solution are second by magnitude after those corresponding to the 4% NaCl + 4% $K_2Cr_2O_7$ solution. This is in consistence with the results of the SSRT testing, showing that 0.1 M NaCl solution can occasionally induce pre-exposure embrittlement. The lowest and close by magnitude corrosion rates and corrosion products weights correspond to the samples exposed to the 4% NaCl + 4% K_2CrO_4 and 5 g/l NaCl + 5 g/l $K_2Cr_2O_7$ solutions, in which no pre-exposure embrittlement has been observed in the present study.

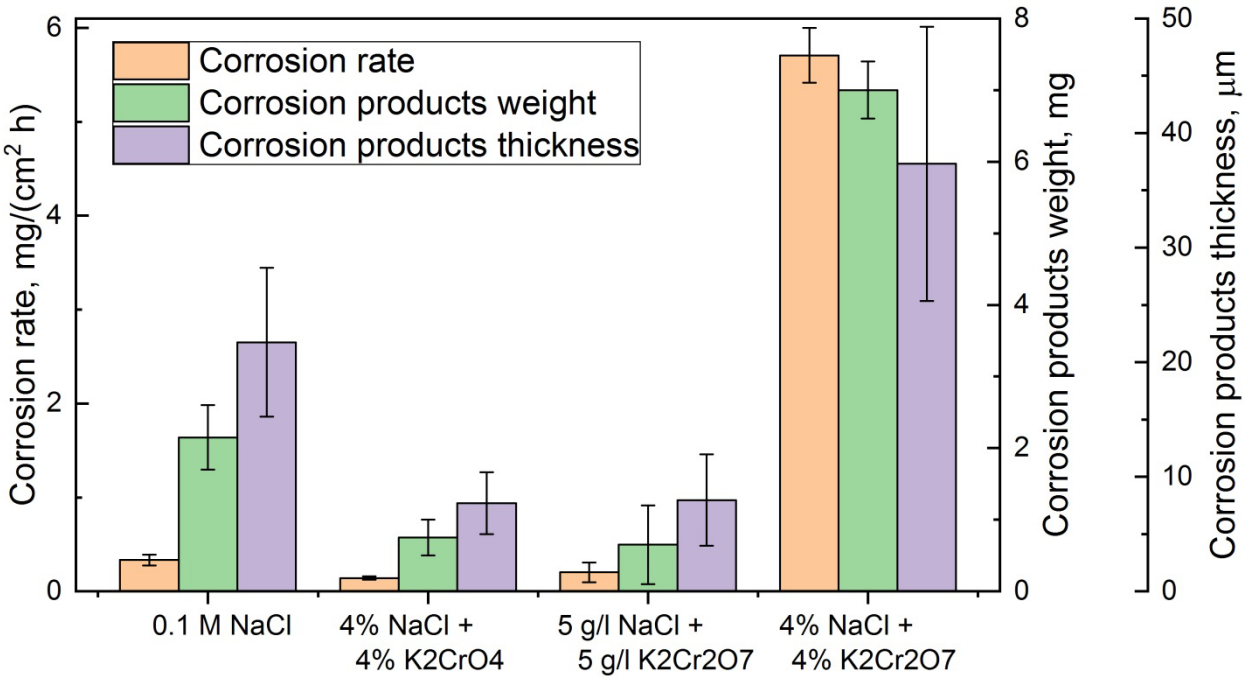

Fig. 14 – The corrosion rate, corrosion products weight and thickness for the alloy ZK60 samples pre-exposed to different corrosion solutions

3.5.Cross-section examination

The SEM images in Figs. 15 and 16 represent the cross-sections of the small samples which were mounted in the epoxy resin immediately after pre-exposure to different corrosive solutions. Figure 15 shows that the thickness of the corrosion products layer, as well as the corrosion damage of the underlying metal, depends strongly on the chemical composition of corrosive media. As expected, the thickest corrosion product film and the most severe corrosion damage correspond to the samples corroded in the 4% NaCl + 4% $K_2Cr_2O_7$ solution, c.f. Fig. 14 and 15d. Nevertheless, the corrosion products film on these samples exhibits a notable variation in thickness due to deep corrosion pits observed all over the side surface of the sample. Corrosion products inside the pits are featured by a dense network of micro-cracks, Fig.16a, which can be interconnected or isolated from each other, Fig.16b. The samples pre-exposed to

three other corrosive solutions demonstrate much less extent of corrosion damage represented by few shallow corrosion pits, such as those shown in Fig. 15b.

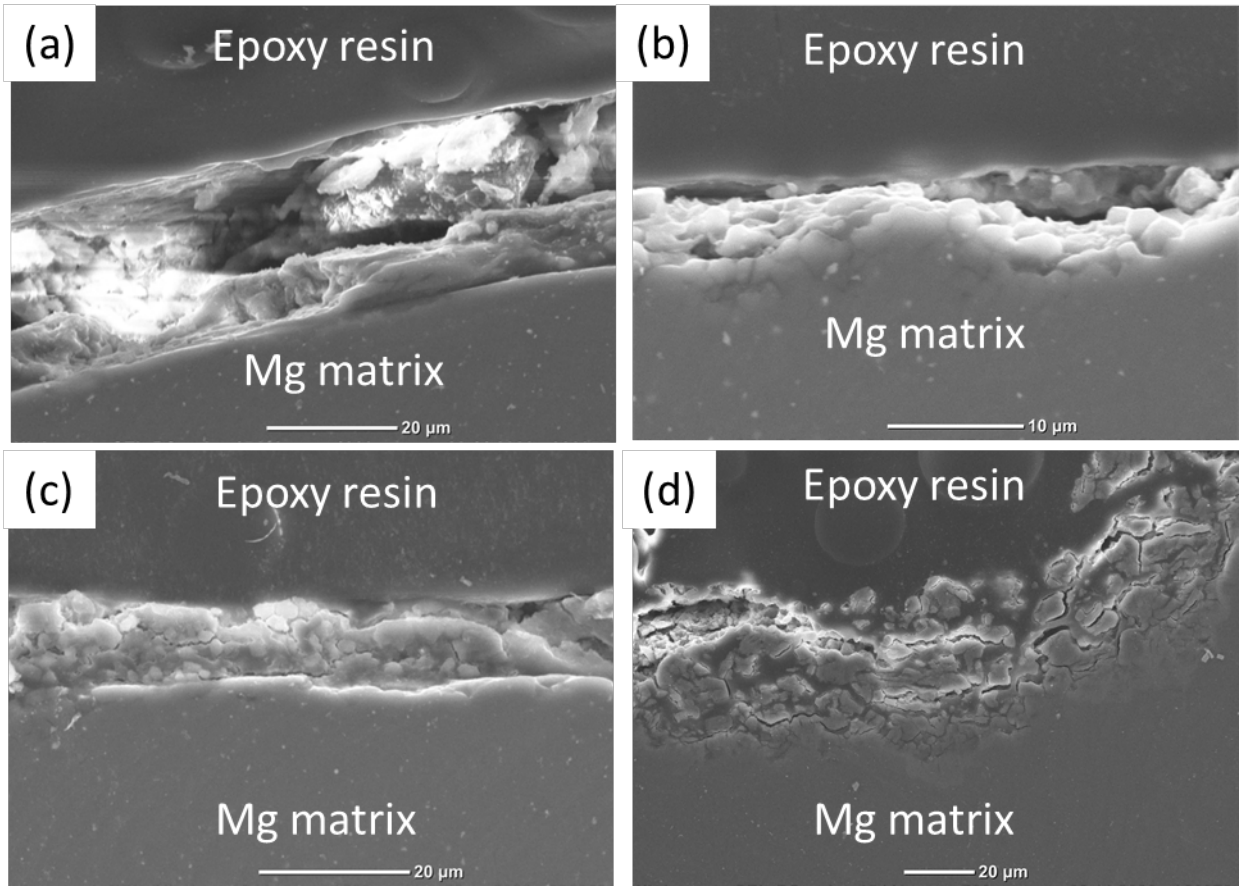

Fig. 15 - The cross-sectional SEM images representing the corrosion products layers on the samples pre-exposed to 0.1 M NaCl – (a), 4% NaCl + 4% K_2CrO_4 – (b), 5 g/l NaCl + 5 g/l $K_2Cr_2O_7$ – (c) and 4% NaCl + 4% $K_2Cr_2O_7$ – (d).

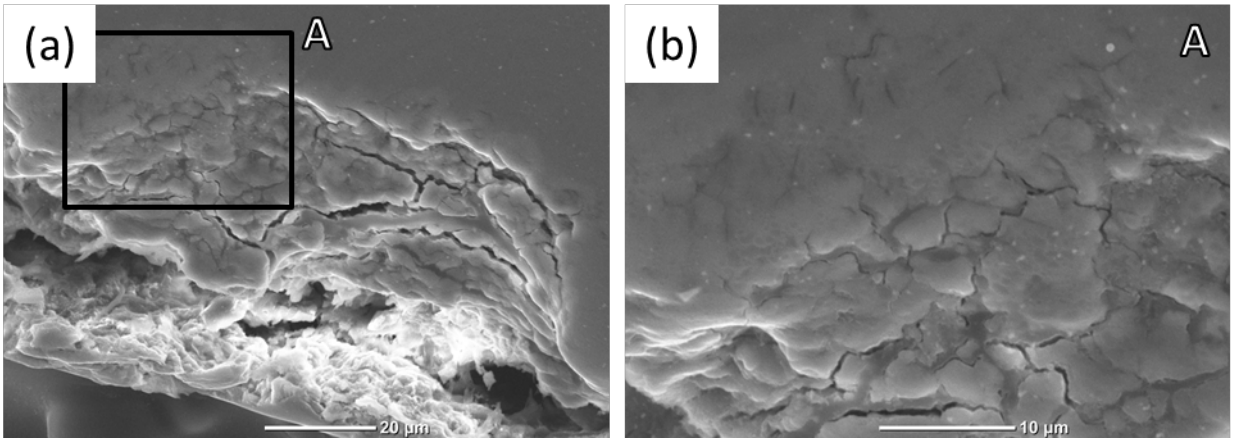

Fig. 16 - The cross-sectional SEM images representing the features of the corrosion products layer and underlying corrosion damage in the sample pre-exposed to 4% NaCl + 4% $K_2Cr_2O_7$.

3.6.Gas-analysis

To clarify the role of hydrogen in the pre-exposure embrittlement observed in the present study, the gas-analysis study has been conducted. It is believed that weakly bonded diffusible hydrogen desorbs from metals, e.g. steels, at the temperatures below 300 °C [38], so it was found reasonable to evaluate the specific concentrations of hydrogen extracting below and above this temperature. The extraction curves represented in Fig. 17 evidence for the extensive evolution of hydrogen from the pre-exposed samples. Several pronounced desorption peaks are distinguished in the temperature range from 25 to 450 °C. It should be noted that at least one peak systematically appears below 300 °C, starting at room temperature.

As follows from Figs. 17 and 18a, the concentration of hydrogen extracted from the samples pre-exposed to the 4% NaCl + 4% $K_2Cr_2O_7$ solution (both below and above 300 °C) is about an order of magnitude higher in comparison to that from the samples pre-exposed to other solutions.

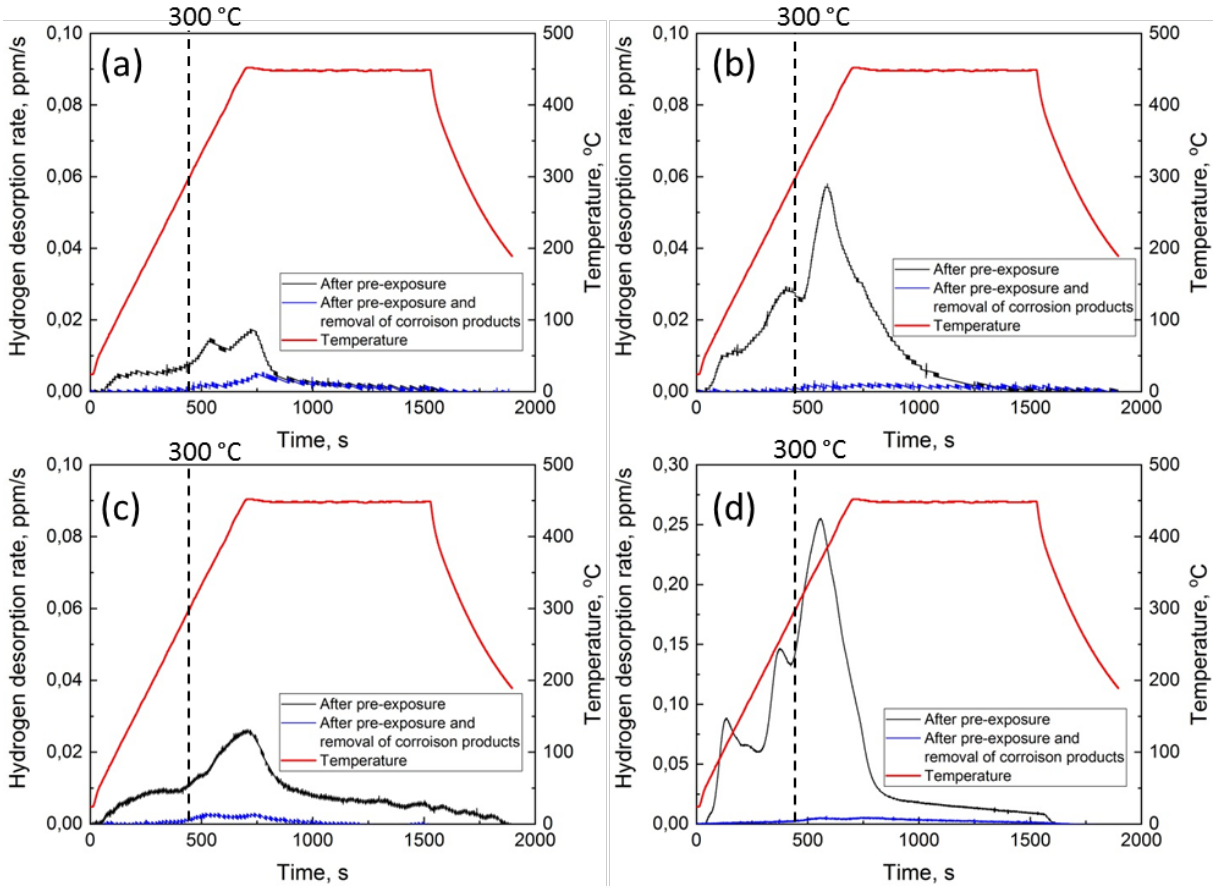

Fig. 17 – The hydrogen desorption rate curves for the samples pre-exposed to 0.1 M NaCl – (a), 4% NaCl + 4% K_2CrO_4 – (b), 5 g/l NaCl + 5 g/l $K_2Cr_2O_7$ – (c) and 4% NaCl + 4% $K_2Cr_2O_7$ – (d).

In harmony with the results of our recent studies [31,32], after the removal of corrosion products, the desorption of hydrogen reduces drastically and occurs primarily above 300 °C, c.f. Fig. 17 and 18b. The highest concentration of hydrogen is observed in the samples pre-exposed to the 4% NaCl + 4% $K_2Cr_2O_7$ solution, being still less than 1 ppm. Thus, this result indicates that only negligible concentration of diffusible hydrogen can exist in the matrix of the pre-exposed samples, regardless of the corrosive solution used. Hydrogen desorbing at temperatures above 300 °C is believed to be mainly associated with the decomposition of the corrosion products such as $Mg(OH)_2$ and MgH_2 [17,32,39]. The precise assignment of each desorption peak to a specific reaction is beyond the scope of the present work and requires a dedicated study.

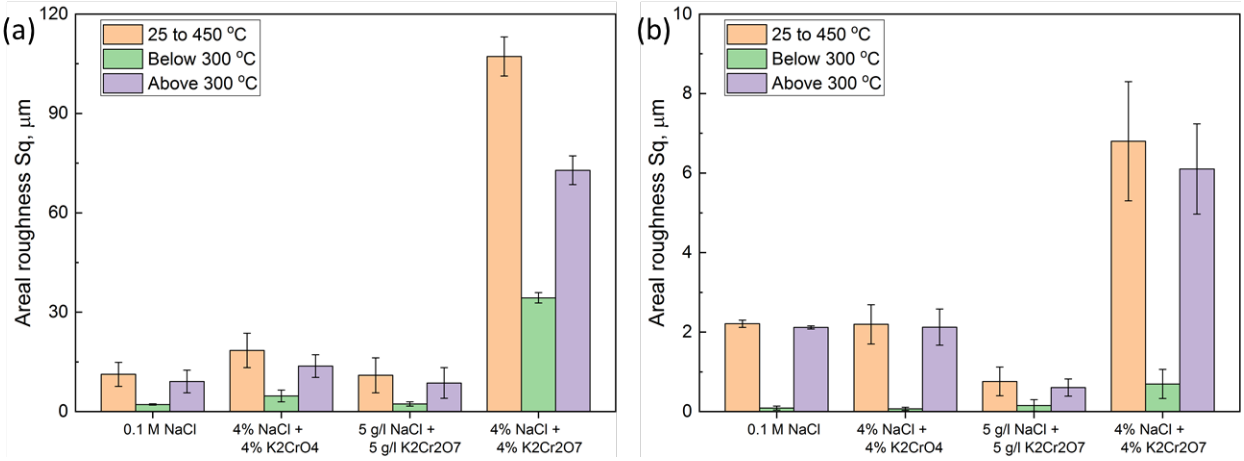

Fig. 18 – Effect of the chemical composition of the corrosion solutions on the concentration of hydrogen desorbed in the different temperature ranges for the pre-exposed samples before – (a) and after – (b) removal of corrosion products.

4. Discussion

The present results convincingly demonstrate that the layer of corrosion products, the properties of which depend on the chemical composition of the corrosive solution, on the surface of the specimen during the pre-exposure in corrosive media exerts a dramatical effect on the mechanical properties and the fracture behaviour of the Mg alloy ZK60. Perhaps, the most striking result is that the removal of corrosion products from the specimen's surface recovers ductility completely, and, in some cases, the ductility even slightly increases. Currently, it is challenging to explain precisely this new finding either based on the present results or from the data reported in the literature. Nevertheless, meaningful insights can be surfaced about the role played by corrosion products in the mechanism of SCC as will be unfolded in what follows.

4.1.Diffusible hydrogen in the matrix

According to the presently dominating viewpoint, the propagation of SCC cracks in magnesium alloys is controlled by diffusible hydrogen accumulated around the crack tip [3,17–20,40]. It is believed that hydrogen produced by the cathodic reaction during the corrosion process is absorbed by the metal. When the external stress is applied, hydrogen tends to diffuse to the triaxial tensile stress region ahead of the crack tip. Being accumulated at the crack tip, hydrogen promotes the propagation of the crack by one of the well-known HE mechanisms such as HEDE, HELP, DHC, etc. Once the crack has advanced through the hydrogen-enriched zone, the crack-arrest and blunting occur until the high enough hydrogen concentration is build up again ahead of the crack. Since the persistent migration of hydrogen towards the crack tip constitutes the necessary condition for the crack growth, the latter occurs in a discontinuous manner, and it is the hydrogen diffusion rate that is the factor limiting the crack growth velocity. The scenario described above mimics the hydrogen-assisted cracking mechanism which has been suggested in several variants by many authors [4,24,28,41] to account for the hydrogen embrittlement or SCC of metallic materials including Mg alloys and steels. As it follows from this scenario the driving factor behind this mechanism is diffusible hydrogen.

The presence of diffusible hydrogen in iron and its alloys is well-documented and evidenced by many experimental techniques such as the thermal desorption spectroscopy (TDS) [42–45], neutron tomography [46,47] and others. Nevertheless, the experimental data on the actual concentration of diffusible hydrogen in Mg alloys are still scarce. The increase in the hydrogen concentration after interaction of Mg alloys with the corrosive environment has been reported in several publications [25,28,48,49]. In these studies, the measurements of hydrogen concentration have been carried out using mainly the melt extraction technique. This method provides information about the total concentration of hydrogen, whereas it is not capable of distinguishing between strongly trapped, chemically bonded and diffusible hydrogen. Furthermore, none of these reports documents the details of the status of corrosion products on the specimen. These details are of crucial methodological importance because the decomposition of corrosion products at elevated temperatures during the gas-analysis can strongly affect the results of hydrogen concentration measurements, giving rise to increasing hydrogen desorption in response to the increasing amount of corrosion products. Indeed, as it was mentioned in the introduction, using the hot-extraction method Merson et al. [31,32] have recently shown that the removal of corrosion products from the surface of the specimens of alloys AZ31, ZK60 and pure Mg subjected to SCC results in the strong reduction of hydrogen evolving from the metal in the temperature interval from 25 to 450 °C. Moreover, it was found that the concentration of

diffusible hydrogen, i.e. hydrogen desorbing at temperatures below 300 °C [38], was negligible in the specimens with removed corrosion products. The present results corroborate those findings and expand upon them by using multiple solutions. As has been shown above, the concentration of diffusible hydrogen in the specimens did not exceed 1 ppm after removal of corrosion products. This was true even for the specimens pre-exposed to the most aggressive 4% NaCl + 4% $K_2Cr_2O_7$ solution, whereas about 33 ppm of hydrogen was desorbed below 300 °C from the as-corroded specimens. Another fact challenging the possibility for the substantial occlusion of diffusible hydrogen in Mg alloys during exposure to corrosive media is that the diffusible hydrogen concentration does not increase with the increasing dislocation density controlled by the amount of pre-strain [32] and the total length of grain boundaries [31], albeit both serve as effective traps of hydrogen as has been documented in ample detail in steels [45,50,51]. It is in place to mention that using the ToF-SIMS technique Brady et al. [50] have shown the possibility of hydrogen absorption in pure Mg and its alloys down to a few tens of micrometers beneath the surface being pre-exposed to H_2O and D_2O. However, with aid from the inelastic neutron scattering vibrational spectrometry it was found that hydrogen was trapped in a molecular form, while the presence of diffusible hydrogen was not witnessed by these techniques.

As previously mentioned, the hypothesis regarding the key role of diffusible hydrogen in SCC of Mg is footed on the results of experiments with the specimens pre-exposed to corrosive media. In several studies, the specimens of pure Mg [33], Mg-Al [28,34,52,53], Mg-Zn-Y-Zr [40] and ZK21 [54] alloys were SSRT-tested in air after soaking in different corrosive solutions for different times. The reduction of ductility and the appearance of brittle regions on the fracture surface of the pre-exposed specimens have been reported in all these studies. Since the aggressive environment was not contacted with the specimens during the SSRT tests, the observed embrittlement was reasonably attributed to diffusible hydrogen absorbed during pre-exposure. The results of the present study ubiquitously show that the removal of corrosion products allows the complete recovery of ductility of the specimens pre-exposed to the different corrosive solutions. If one assumes that embrittlement is caused by diffusible hydrogen retaining in the matrix of the pre-exposed specimens, then the only explanation for the effect of removing corrosion products is that diffusible hydrogen is fully evolved from the specimen after removing corrosion products. Indeed, the thick corrosion product film composed of Mg hydroxide, oxide and hydride and other components may probably serve as a barrier for the hydrogen desorption from the matrix. It was shown that the layer of $Mg(OH)_2$ [33] as well as MgH_2 [55,56] deposited on the surface of Mg prevents the absorption of hydrogen. However, the time gap between the removal of corrosion products and the beginning of mechanical testing in the present study was

very short (less than 5 min). It is quite doubtful that such a short time is enough for the complete desorption of hydrogen from the metal. The considerable uncertainty exists in the literature regarding the magnitude of the diffusion coefficient, D_H, of hydrogen in Mg and its alloys [17]. The reported values of D_H at room temperature varied broadly from 10^{-9} [3] down to 10^{-20} m^2/s [55], depending on the evaluation method, material, etc. The upper bound estimates are obtained by extrapolation from high-temperature data [3]. The D_H values assessed in this way, e.g. for steels, are commonly greatly overestimated because, at low temperatures, the hydrogen diffusion rate is significantly affected by H-trapping sites [57,58]. If diffusible hydrogen is not able to evolve from the pre-exposed specimen before SSRT testing, then either this hydrogen does not induce embrittlement, or it merely does not exist in the metal in the sufficient amount. The latter explanation is congruent with the results of the gas-analysis conducted in the present work and our recent studies [31,32], which revealed the negligible concentration of diffusible hydrogen in the metallic matrix of ZK60 alloy subjected to SCC as well as to corrosion in different aggressive media. The corollary from these observations is that the absorption of hydrogen during pre-exposure to corrosive media is likely quite limited. Perhaps, this is due to the formation of the surface barrier hydride layer which is not permeable for hydrogen atoms. One may reasonably suppose that the 1.5 h pre-exposure time used in the present study is insufficient for deep penetration of hydrogen into the bulk material. The pre-exposure process exceeding usually 4 h or so has been widely used by many researchers [28,34,40,52–54]. Undoubtedly, the effect of pre-exposure time requires additional investigations. The new data gained in the present work highlight this need which will be addressed in our forthcoming publication. Nevertheless, as for now, the results of the present work undeniably show that even such a short pre-exposure time can result in the significant embrittlement effect, which can be fully eliminated by removal of corrosion products. Thereby, there might be another factor inducing embrittlement without reference to diffusible hydrogen in the matrix.

4.2.Hydrogen and retained corrosive solution in corrosion products

The healing effect produced by removing corrosion products suggests that the embrittling agent can be located preferentially in the corrosion product layer. Such embrittling agents can include diffusible or molecular hydrogen. Alternatively, retained liquid corrosive media can also serve as an embrittling agent. These agents can sit either at the interface between the metal and the thick corrosion product layer or within the discontinuities in the corrosion products. The presence of hydrogen in corrosion products is evidently supported in the present study by the results of the gas-analysis unveiling significant hydrogen desorption from the specimens covered by corrosion products in the temperature range from 25 to 300 °C. Hydrogen desorbing at these

temperatures can be partly associated with atomic or molecular hydrogen retaining in the corrosion products. Both atomic and molecular hydrogen may adsorb at the metallic surface of the specimen, thus causing hydrogen-assisted cracking through the AIDE mechanism. The interaction of Mg surface with hydrogen can also result in the formation of brittle hydrides, which can activate the crack growth through the DHC mechanism. The relationship between hydrogen sitting in the corrosion products layer and the pre-exposure embrittlement is further supported by the observation that the greatest concentration of hydrogen desorbed below 300 °C is measured in the specimens pre-exposed to the 4% NaCl + 4% $K_2Cr_2O_7$ solution causing the most severe embrittlement effect.

Although the direct evidence for the presence of liquid corrosive media under corrosion products has not been reported up to date, one should not deny such a possibility a priory. The liquid phase might retain within the corrosion products layer containing numerous cracks and discontinuities as is observed on the cross-sections of the samples pre-exposed to 4% NaCl + 4% $K_2Cr_2O_7$. The retained liquid, if exists, gives way for corrosion to occur beneath the corrosion products even after extraction of the specimen from the corrosive solution. This would produce hydrogen, which could be responsible for low-temperature desorption peaks detected by the gas-analysis. Liquid corrosive media interacting with the surface should result in SCC during SSRT testing of the pre-exposed specimen in the same way as it does during routine testing of the initial specimens in corrosive media.

If the embrittlement of the pre-exposed specimens is caused by hydrogen or liquid corrosive solution contained in corrosion products or at the interface between the corrosion products film and the surface of the metal, it is reasonable to anticipate the lack of embrittlement after removal of the corrosion products. On the other hand, the presence of embrittling agents in the pre-exposed specimens is only expected if the layer of corrosion products covers the surface totally, is thick enough, and if it forms quickly enough to seal these agents. These prerequisites conform to the results of the present study. As we discussed above, the severe embrittlement is persistently observed only when the specimens were pre-exposed to the 4% NaCl + 4% $K_2Cr_2O_7$ solution where the thick corrosion products film covered the entire surface as is evidenced by the microscopic cross-section examination and weight measurements. The specimens pre-exposed to other solutions exhibited only partial coverage by corrosion products forming thinner layers, giving rise to lesser or no embrittlement.

The presence of the embrittling agent is also suggested by the results of the side and fracture surface analysis. The side surface examination shows that the corrosion products film on

the surface of the specimens is very brittle. This is evidenced by numerous brittle cracks, which, presumably, initiated in the corrosion layer and then propagated towards the bulk, producing brittle regions on the fracture surface. However, in the specimens, which demonstrate insignificant embrittlement after pre-exposure, the cracks do not grow deep, producing just the featureless regions covered by corrosion products on the fracture surface. These cracks are blunted and strongly yawned, apparently due to considerable plasticity. In contrast, in the specimens, which do exhibit embrittlement, the cracks are much less opened, and the sizeable brittle area is seen on the fracture surface. The featureless regions with the corrosion products, in this case, are found only in the vicinity of the side surface, while closer to the central part of the fracture surface one finds cleavage and fluted features. In our opinion, this fact suggests the presence of the embrittling agent, which prevents crack blunting in the strongly embrittled specimens, thus facilitating the brittle crack growth. Presumably, in the pre-exposed specimens which exhibit less or no embrittlement the embrittling agent is absent, giving way to crack blunting. The nature of the featureless regions, which have been systematically observed on the fracture surface, is to be revealed in further studies. However, one may suppose that these regions develop from the corrosion pits, which were formed during the pre-exposure process, and which were considered as the primary initiation points for the SCC cracks by other investigators [18,19,33,53].

Despite the provisional character of the present discussion, the hypothesis regarding the presence of hydrogen or liquid corrosion media in the corrosion products layer requires a thorough verification, and this will be the scope of our further studies.

4.3.Corrosion product film-induced stress

It has been well-established that the mechanical and fracture behaviour of many metallic materials is affected by the corrosion products film itself in a mechanistic way due to the so-called "corrosion product film-induced stress", which refers to the stress induced in the metallic substrate to balance the residual stress in the corrosion product film [59]. It has been shown that this stress, which is commonly tensile and maximal at the interface between the corrosion products film and the metallic substrate, enhances SCC in Ti [60], copper alloys [59,61,62], low-carbon [63] and stainless steels [64]. For example, Asawa et al. [64] showed that the repeated removal of corrosion products from the specimens of Cu alloyed 304 stainless steel subjected to the constant load in 1M H_2SO_4 solution resulted in a considerable reduction of the number and the length of SCC cracks. The authors concluded that the corrosion products film governs the SCC behaviour of the alloy by accelerating both the crack initiation and propagation stages.

Although for Mg alloys this phenomenon has not been considered so far to the authors' best knowledge, the results of the present study suggest that SCC of these materials can also be enhanced by corrosion product film-induced stress. The correlation revealed between the susceptibility to the pre-exposure embrittlement and the properties of the corrosion products film indicates the likeliness of such a process to occur. It is still unclear whether it is the only factor (or the dominant factor) controlling SCC of the pre-exposed specimens or it cooperates with the embrittling agents such as those mentioned above. To distinguish between the above-discussed scenarios and to assess the contributions from hydrogen, liquid embrittlement or the corrosion product film-induced stress, and, possibly, to give priority to one of them, the strain rate effect on the mechanical properties has to be examined in the pre-exposed specimens. In contrast to the hydrogen or liquid-induced embrittlement the film-induced effect should not be time- or strain rate dependent. To the authors best knowledge, there is only one paper where the experiments of this kind have been conducted [28]. The authors have found that embrittlement of the pre-exposed specimens of the Al-Mg alloy was eliminated as the strain rate increased from 10^{-4} to 10^{-2} s^{-1}, thus suggesting that the time-dependent mechanism is essential in the embrittlement process. Nevertheless, the mechanical response observed in [28] was not typical for hydrogen embrittlement, because of the long plateau region from 10^{-4} to $5 \cdot 10^{-2}$ s^{-1}, where the embrittlement was pronounced, followed by the steep increase and complete recovery of mechanical properties at higher strain rates. Thereby, the present results highlight the need for the additional study of the effect of the strain rate on the mechanical behaviour of the pre-exposed Mg specimens to unveil the role of the corrosion product film-induced stress in the SCC mechanism in magnesium alloys.

4.4.Irreversible corrosion damage

The discussion would be incomplete without touching the irreversibility of the corrosion-induced damage. The deterioration of mechanical properties of Mg alloys due to the irreversible corrosion damage induced by pre-exposure to corrosive media has been reported by several researchers [28,34,54]. As has been demonstrated, the removal of corrosion products results in the complete recovery of ductility, whereas the ultimate tensile strength is generally slightly lower than that of the reference specimens tested in air. The most notable irreversible UTS reduction occurs in the specimens pre-exposed to 4% NaCl + 4% $K_2Cr_2O_7$. The measurements of the corrosion rate and roughness have conclusively shown that the corrosion damage produced by this solution is an order of magnitude higher than in other solutions. Since no brittle features are observed on the fracture surface of the specimens with removed corrosion products, the irreversible reduction of UTS is attributed to the decrease in the cross-section area due to the

extensive corrosion damage. It is also found that after removal of corrosion products, the elongation of the pre-exposed specimens is even higher than that of the reference specimens. This effect can be probably associated with the removing of the thin surface layer of the specimen during corrosion processes. Since the surface layer of the machined specimens contains stress risers and residual stresses at the surface, the removal of this layer can positively influence the ductility of the specimens.

As a final note, let us emphasise that employing different corrosive solutions in this study, we aimed primarily at verifying our key finding – the recovery of mechanical properties after removal of corrosive products from the surface. The generality of this result has been undoubtedly confirmed for several solutions resulting in notably different corrosion rates, and, thus, the goal has been met. Besides, the present results concur with those from multiple studies showing that the chemical composition of the corrosive solution exerts a strong influence on the embrittlement phenomenon in Mg alloys, c.f. [65,66]. Details of the chemical interactions between the metal surface and the solution are, however, left beyond the scope of the present work, and have yet to be clarified.

5. Summary and conclusions

We have demonstrated that the removal of corrosion products exerts a strong recovering effect on the mechanical response of the specimens of ZK60 alloy pre-exposed to the different corrosion solutions. The complex analysis of the results of SSRT testing, microscopic examination of the side and fracture surfaces offered new insights on the nature of SCC in Mg alloys and uncovered the critical role of corrosion products in this phenomenon. Experimental findings are summarised as follows.

1. The specimens of the alloy ZK60 SSRT tested in different NaCl-based solutions suffer from severe SCC leading to a remarkable drop in mechanical properties, the appearance of brittle fracture surfaces and brittle secondary cracks on the side surface. The severity of SCC depends on the composition of the corrosive solution. In general, the SCC of the alloy is enhanced with (i) the addition of passivating agents such as dichromate or chromate into the corrosive solution, (ii) the simultaneous increase of concentrations of both NaCl and $K_2Cr_2O_7$, (iii) the addition of dichromate instead of chromate.
2. The pre-exposure of the alloy ZK60 to corrosive media can cause the embrittlement which manifests itself by the reduction in tensile ductility and strength during

SSRT testing in air accompanied by the appearance of brittle regions on the fracture surface. The degree of the pre-exposure embrittlement increases with the weight, thickness and hiding power of corrosion products deposited on the surface. In turn, these characteristics of the corrosion product film depend on the chemical composition of the corrosive solution and increase with increasing corrosion rate of the alloy. The most expansive corrosion products and, concurrently, the most severe embrittlement phenomenon are observed in the specimens pre-exposed to the 4% NaCl + 4% $K_2Cr_2O_7$ solution.

3. Pre-exposure to corrosive media results in the appearance of numerous secondary cracks on the side surface and the corresponding featureless regions covered with corrosion products on the fracture surface of SSRT tested specimens, regardless of the chemical composition of the corrosive solution. However, in the specimens with the thin corrosion products film, these cracks do not propagate deep into the specimen interior. Neither they cause substantial embrittlement, while in the specimens with the dense corrosion products film the cracks substantially advance during SSRT testing in air, producing large brittle areas on the fracture surface, represented by facets with cleavage and fluted morphology.

4. The concentration of diffusible hydrogen in the ZK60 alloy matrix after pre-exposure to corrosive solutions is negligible. Therefore, diffusible hydrogen cannot be blamed responsible for the pre-exposure embrittlement. In contrast, large volume of hydrogen is contained in the corrosion products layer deposited on the specimen's surface.

5. The embrittlement induced by pre-exposure of the specimens to corrosive media can be fully eliminated by to the removal of corrosion products from the specimen’s surface before SSRT testing in air, provided the cross-section area is not affected by irreversible corrosion damage.

Thus, the corollary from these observations is that the corrosion products depositing on the surface of ZK60 alloy specimens during pre-exposure to corrosive media play a crucial role in the embrittlement mechanism of Mg-based alloys.

The main thrust of the present work is that the healing effect produced by the removal of corrosion product layer challenges the significance of diffusible hydrogen in the embrittlement induced by pre-exposure of magnesium-based alloys in corrosive media. The factors, which can potentially affect the embrittlement process caused by pre-exposure to corrosive media, include (i) hydrogen or liquid corrosive media sealed at the interface between the substrate and corrosion products or within the corrosion product layer; (ii) the corrosion product film-induced stress, (iii) irreversible corrosion damage.

Acknowledgements

Financial support from the Russian Science Foundation through the grant-in-aid No. 18-19-00592 is gratefully appreciated.

References

[1] V.S. Raja, T. Shoji, eds., Stress Corrosion Cracking. Theory and Practice, 2011.

[2] A. Atrens, N. Winzer, W. Dietzel, Stress corrosion cracking of magnesium alloys, Adv. Eng. Mater. 13 (2011) 11–18. doi:10.1002/adem.200900287.

[3] A. Atrens, W. Dietzel, P. Bala Srinivasan, N. Winzer, M. Bobby Kannan, Stress corrosion cracking (SCC) of magnesium alloys, in: Stress Corros. Crack., Elsevier, 2011: pp. 341–380. doi:10.1533/9780857093769.3.341.

[4] N. Winzer, A. Atrens, G. Song, E. Ghali, W. Dietzel, K.U. Kainer, et al., A critical review of the Stress Corrosion Cracking (SCC) of magnesium alloys, Adv. Eng. Mater. 7 (2005) 659–693. doi:10.1002/adem.200500071.

[5] T.T.T. Trang, J.H. Zhang, J.H. Kim, A. Zargaran, J.H. Hwang, B.C. Suh, et al., Designing a magnesium alloy with high strength and high formability, Nat. Commun. 9 (2018). doi:10.1038/s41467-018-04981-4.

[6] A. Vinogradov, V.N. Serebryany, S. V. Dobatkin, Tailoring microstructure and properties of fine grained magnesium alloys by severe plastic deformation, Adv. Eng. Mater. 20 (2018) 1–22. doi:10.1002/adem.201700785.

[7] K.K. Sankaran, R.S. Mishra, Magnesium Alloys, in: Metall. Des. Alloy. with Hierarchical Microstruct., Elsevier, 2017: pp. 345–383. doi:10.1016/B978-0-12-812068-2.00007-2.

[8] B. Landkof, Magnesium Alloys and their Applications, Wiley, Weinheim, FRG, 2000. doi:10.1002/3527607552.

[9] W.J. Joost, P.E. Krajewski, Towards magnesium alloys for high-volume automotive applications, Scr. Mater. 128 (2017) 107–112. doi:10.1016/j.scriptamat.2016.07.035.

[10] M.K. Kulekci, Magnesium and its alloys applications in automotive industry, Int. J. Adv.

Manuf. Technol. 39 (2008) 851–865. doi:10.1007/s00170-007-1279-2.

[11] B. Landkof, Magnesium Applications in Aerospace and Electronic Industries, in: Magnes. Alloy. Their Appl., Wiley-VCH Verlag GmbH & Co. KGaA, Weinheim, FRG, 2006: pp. 168–172. doi:10.1002/3527607552.ch28.

[12] A. Vinogradov, E. Vasilev, V.I. Kopylov, M. Linderov, A. Brilevesky, D. Merson, High performance fine-grained biodegradable Mg-Zn-Ca alloys processed by severe plastic deformation, Metals (Basel). 9 (2019). doi:10.3390/met9020186.

[13] Y. Yang, C. He, Dianyu E, W. Yang, F. Qi, D. Xie, et al., Mg bone implant: Features, developments and perspectives, Mater. Des. 185 (2020) 108259. doi:10.1016/j.matdes.2019.108259.

[14] U. Riaz, I. Shabib, W. Haider, The current trends of Mg alloys in biomedical applications—A review, J. Biomed. Mater. Res. - Part B Appl. Biomater. 107 (2019) 1970–1996. doi:10.1002/jbm.b.34290.

[15] R. Radha, D. Sreekanth, Insight of magnesium alloys and composites for orthopedic implant applications – a review, J. Magnes. Alloy. 5 (2017) 286–312. doi:10.1016/j.jma.2017.08.003.

[16] D. Merson, A. Brilevsky, P. Myagkikh, A. Tarkova, A. Prokhorikhin, E. Kretov, et al., The functional properties of Mg-Zn-X biodegradable magnesium alloys, Materials (Basel). 13 (2020) 1–18. doi:10.3390/ma13030544.

[17] M. Kappes, M. Iannuzzi, R.M. Carranza, Hydrogen Embrittlement of Magnesium and Magnesium Alloys: A Review, J. Electrochem. Soc. 160 (2013) C168–C178. doi:10.1149/2.023304jes.

[18] N. Winzer, A. Atrens, W. Dietzel, G. Song, K.U. Kainer, Fractography of stress corrosion cracking of Mg-Al alloys, Metall. Mater. Trans. A Phys. Metall. Mater. Sci. 39 A (2008) 1157–1173. doi:10.1007/s11661-008-9475-8.

[19] N. Winzer, A. Atrens, W. Dietzel, V.S. Raja, G. Song, K.U. Kainer, Characterisation of stress corrosion cracking (SCC) of Mg – Al alloys, Mater. Sci. Eng. A. 48 (2008) 339-351.

[20] W. Dietzel, Hydrogen Embrittlement of Biodegradable Magnesium, Solid State Phenom. 225 (2014) 71–76. doi:10.4028/www.scientific.net/SSP.225.71.

[21] D.B. Prabhu, S. Dhamotharan, G. Sathishkumar, P. Gopalakrishnan, K.R. Ravi, Stress corrosion cracking of biodegradable Mg-4Zn alloy in simulated body fluid at different strain rates – A fractographic investigation, Mater. Sci. Eng. A. 730 (2018) 223–231. doi:10.1016/j.msea.2018.06.002.

[22] M. Nagumo, Fundamentals of Hydrogen Embrittlement, Springer Singapore, Singapore, 2016. doi:10.1007/978-981-10-0161-1.

[23] I.M. Robertson, P. Sofronis, A. Nagao, M.L. Martin, S. Wang, D.W. Gross, et al., Hydrogen Embrittlement Understood, Metall. Mater. Trans. A. 46 (2015) 2323–2341. doi:10.1007/s11661-015-2836-1.

[24] S.P. Lynch, Hydrogen embrittlement phenomena and mechanisms, Corros. Rev. 30 (2012) 63–133. doi:10.1515/corrrev-2012-0502.

[25] L.F. Zhou, Z.Y. Liu, W. Wu, X.G. Li, C.W. Du, B. Jiang, Stress corrosion cracking behavior of ZK60 magnesium alloy under different conditions, Int. J. Hydrogen Energy. 42 (2017) 26162–26174. doi:10.1016/j.ijhydene.2017.08.161.

[26] F. Tuchscheerer, L. Krüger, Hydrogen-induced embrittlement of fine-grained twin-roll cast AZ31 in distilled water and NaCl solutions, J. Mater. Sci. 50 (2015) 5104–5113. doi:10.1007/s10853-015-9064-3.

[27] S.P. Lynch, P. Trevena, Stress corrosion cracking and liquid metal embrittlement in pure magnesium, Corrosion. 44 (1988) 113–124.

[28] D.G. Chakrapani, E.N. Pugh, Hydrogen embrittlement in a Mg-Al alloy, Metall. Trans. A. 7 (1976) 173–178. doi:10.1007/BF02644454.

[29] D.G. Chakrapani, E.N. Pugh, On the Fractography of Transgranular Stress Corrosion Failures in a Mg-Al Alloy, Corrosion. 31 (1975) 247–252. doi:10.5006/0010-9312-31.7.247.

[30] D.G. Chakrapani, E.N. Pugh, The transgranular SCC of a Mg-Al alloy: Crystallographic, fractographic and acoustic-emission studies, Metall. Trans. A. 6 (1975) 1155–1163. doi:10.1007/BF02658523.

[31] E.D. Merson, V.A. Poluyanov, P.N. Myagkikh, D.L. Merson, A.Y. Vinogradov, Effect of grain size on mechanical properties and hydrogen occluding capacity of pure magnesium and alloy MA14 subjected to stress-corrosion cracking, Lett. Mater. 10 (2020) 94–99.

doi:10.22226/2410-3535-2020-1-94-99.

[32] E. Merson, P. Myagkikh, V. Poluyanov, D. Merson, A. Vinogradov, On the role of hydrogen in stress corrosion cracking of magnesium and its alloys: Gas-analysis study, Mater. Sci. Eng. A. 748 (2019) 337–346. doi:10.1016/j.msea.2019.01.107.

[33] R.S. Stampella, R.P.M. Procter, V. Ashworth, Environmentally-induced cracking of magnesium, Corros. Sci. 24 (1984) 325–337. doi:10.1016/0010-938X(84)90017-9.

[34] M. Kappes, M. Iannuzzi, R.M. Carranza, Pre-Exposure embrittlement and stress corrosion cracking of magnesium alloy AZ31B in chloride solutions, Corrosion. 70 (2014) 667–677. doi:10.5006/1172.

[35] E. Merson, V. Poluyanov, P. Myagkikh, D. Merson, A. Vinogradov, Fractographic features of technically pure magnesium, AZ31 and ZK60 alloys subjected to stress corrosion cracking, Mater. Sci. Eng. A. 772 (2020) 138744. doi:10.1016/j.msea.2019.138744.

[36] L. Fairman, J.M. West, Stress corrosion cracking of a magnesium aluminium alloy, Corros. Sci. 5 (1965) 711–716. doi:10.1016/S0010-938X(65)80027-0.

[37] E.D. Merson, P.N. Myagkikh, V.A. Poluyanov, D.L. Merson, A. Vinogradov, Quasi-cleavage hydrogen-assisted cracking path investigation by fractographic and side surface observations, Eng. Fract. Mech. 214 (2019) 177–193. doi:10.1016/j.engfracmech.2019.04.042.

[38] A. Laureys, T. Depover, R. Petrov, K. Verbeken, Influence of sample geometry and microstructure on the hydrogen induced cracking characteristics under uniaxial load, Mater. Sci. Eng. A. 690 (2017) 88–95. doi:10.1016/j.msea.2017.02.094.

[39] E.A. Evard, I.E. Gabis, M.A. Murzinova, Kinetics of hydrogen liberation from stoichiometric and nonstoichiometric magnesium hydride, Mater. Sci. 43 (2007) 620–633. doi:10.1007/s11003-008-9002-5.

[40] S.D. Wang, D.K. Xu, B.J. Wang, L.Y. Sheng, E.H. Han, C. Dong, Effect of solution treatment on stress corrosion cracking behavior of an as-forged Mg-Zn-Y-Zr alloy, Sci. Rep. 6 (2016) 1–12. doi:10.1038/srep29471.

[41] N. Winzer, A. Atrens, W. Dietzel, G. Song, K.U. Kainer, Evaluation of the delayed hydride cracking mechanism for transgranular stress corrosion cracking of magnesium

alloys, Mater. Sci. Eng. A. 466 (2007) 18–31. doi:10.1016/j.msea.2007.03.020.

[42] M. Nagumo, K. Takai, N. Okuda, Nature of hydrogen trapping sites in steels induced by plastic deformation, J. Alloys Compd. 293 (1999) 310–316. doi:10.1016/S0925-8388(99)00322-9.

[43] F.G. Wei, K. Tsuzaki, Quantitative analysis on hydrogen trapping of TiC particles in steel, Metall. Mater. Trans. A. 37A (2006) 331–353. doi:10.1007/s11661-006-0004-3.

[44] C. V. Tapia-Bastidas, A. Atrens, E.M.A. Gray, Thermal desorption spectrometer for measuring ppm concentrations of trapped hydrogen, Int. J. Hydrogen Energy. 43 (2018) 7600–7617. doi:10.1016/j.ijhydene.2018.02.161.

[45] J.-Y. Lee, S.M. Lee, Hydrogen trapping phenomena in metals with B.C.C. and F.C.C. crystals structures by the desorption thermal analysis technique, Surf. Coatings Technol. 28 (1986) 301–314. doi:http://dx.doi.org/10.1016/0257-8972(86)90087-3.

[46] A. Griesche, E. Dabah, T. Kannengiesser, N. Kardjilov, A. Hilger, I. Manke, Three-dimensional imaging of hydrogen blister in iron with neutron tomography, Acta Mater. 78 (2014) 14–22. doi:10.1016/j.actamat.2014.06.034.

[47] B. Pfretzschner, T. Schaupp, A. Griesche, Hydrogen in metals visualized by neutron imaging, CORROSION. (2019) 3104. doi:10.5006/3104.

[48] M. Sozańska, A. Mościcki, Investigation of the Susceptibility of the WE54 Magnesium-Based Alloy to Stress Corrosion Cracking, J. Mater. Eng. Perform. 29 (2020) 949–963. doi:10.1007/s11665-019-04550-w.

[49] M. Sozańska, A. Mościcki, T. Czujko, The characterization of stress corrosion cracking in the AE44 magnesium casting alloy using quantitative fractography methods, Materials (Basel). 12 (2019) 1–16. doi:10.3390/MA12244125.

[50] W.Y. Choo, J.Y. Lee, Effect of cold working on the hydrogen trapping phenomena in pure iron, Metall. Trans. A. 14 (1983) 1299–1305. doi:10.1007/BF02664812.

[51] E.D. Merson, P.N. Myagkikh, G. V. Klevtsov, D.L. Merson, A. Vinogradov, Effect of equal-channel angular pressing (ECAP) and current density of cathodic hydrogen charging on hydrogen trapping in the low-alloy steel, Lett. Mater. 10 (2020) 152–157.

[52] R.G. Song, C. Blawert, W. Dietzel, A. Atrens, A study on stress corrosion cracking and

hydrogen embrittlement of AZ31 magnesium alloy, Mater. Sci. Eng. A. 399 (2005) 308–317. doi:10.1016/j.msea.2005.04.003.

[53] M. Bobby Kannan, W. Dietzel, Pitting-induced hydrogen embrittlement of magnesium-aluminium alloy, Mater. Des. 42 (2012) 321–326. doi:10.1016/j.matdes.2012.06.007.

[54] S. Jafari, R.K.S. Raman, C.H.J. Davies, Stress corrosion cracking of an extruded magnesium alloy (ZK21) in a simulated body fluid, Eng. Fract. Mech. 201 (2018) 47–55. doi:10.1016/j.engfracmech.2018.09.002.

[55] P. Spatz, H.A. Aebischer, A. Krozer, L. Schlapbach, The Diffusion of H in Mg and the Nucleation and Growth of Mgh2 In Thin Films, Zeitschrift Fur Phys. Chemie. 181 (1993) 393–397. doi:10.1524/zpch.1993.181.Part_1_2.393.

[56] A. Krozer, B. Kasemo, Thermodynamics and Kinetics of the H/Mg System at Low Pressures and Temperatures, Zeitschrift Fur Phys. Chemie. 164 (1989) 1257–1258. doi:10.1524/zpch.1989.164.Part_2.1257.

[57] W.Y. Choo, J. Lee, Hydrogen trapping phenomena in carbon steel, J. Mater. Sci. 17 (1982) 1930–1938. doi:10.1007/BF00540409.

[58] A. Turnbull, Hydrogen diffusion and trapping in metals, in: R.P. Gangloff, B.P. Somerday (Eds.), Gaseous Hydrog. Embrittlement Mater. Energy Technol. Vol. 2 Mech. Model. Futur. Dev., Woodhead Publishing Limited, Philadelphia, 2012: pp. 89–128. doi:10.1533/9780857095374.1.89.

[59] W. Wang, Z. Zhang, X. Ren, Y. Guan, Y. Su, Corrosion product film-induced stress facilitates stress corrosion cracking, Sci. Rep. 5 (2015) 1–11. doi:10.1038/srep10579.

[60] X.Z. Guo, K.W. Gao, W.Y. Chu, L.J. Qiao, Correlation between passive film-induced stress and stress corrosion cracking of α-Ti in a methanol solution various potentials, Mater. Sci. Eng. A. 346 (2003) 1–7. doi:10.1016/S0921-5093(02)00529-4.

[61] X.S. Du, Y.J. Su, C. Zhang, J.X. Li, L.J. Qiao, W.Y. Chu, et al., Pre-strain enhances film rupture to promote SCC of brass in Mattsson's solution - A proposal for a film-rupture-induced SCC mechanism, Corros. Sci. 69 (2013) 302–310. doi:10.1016/j.corsci.2012.11.043.

[62] X. Guo, K. Gao, L. Qiao, W. Chu, Stress corrosion cracking relation with dezincification layer-induced stress, Metall. Mater. Trans. A Phys. Metall. Mater. Sci. 32 (2001) 1309–

1312. doi:10.1007/s11661-001-0221-8.

[63] X.S. Du, Y.J. Su, J.X. Li, L.J. Qiao, W.Y. Chu, Stress corrosion cracking of A537 steel in simulated marine environments, Corros. Sci. 65 (2012) 278–287. doi:10.1016/j.corsci.2012.08.025.

[64] M. Asawa, A. Devasenapathi, M. Fujisawa, Effect of corrosion product layer on SCC susceptibility of copper containing type 304 stainless steel in 1 M H2SO4, Mater. Sci. Eng. A. 366 (2004) 292–298. doi:10.1016/j.msea.2003.08.112.

[65] B. Wilson, J.R. McDermid, J.R. Kish, Technical note: Screening of salt fog environments for Mg alloy stress corrosion cracking susceptibility, Corrosion. 73 (2017) 1300–1305. doi:10.5006/2501.

[66] K. Ebtehaj, D. Hardie, R.N. Parkins, The influence of chloride-chromate solution composition on the stress corrosion cracking of a Mg-Al alloy, Corros. Sci. 28 (1988) 811–821. doi:10.1016/0010-938X(88)90119-9.